SPATIAL AND METABOLIC REQUIREMENTS OF MITOCHONDRIA DURING MDA-MB-231 CELL MIGRATION *IN VITRO*

By

Justin Lawrence

A Thesis Submitted in Partial Fulfillment

of the Requirements for the Degree of

Master of Science in Biology

Austin Peay State University

May 2020

Thesis Committee:

Dr. Sarah Lundin Schiller, Committee Chair

Dr. Amy Thompson

Dr. Gilbert Pitts

To the College of Graduate Studies:

We are submitting a thesis written by Justin Lawrence entitled “Spatial and metabolic requirements of mitochondria during MDA-MB-231 cell migration *in vitro*”. We have examined the final copy of this thesis for form and content. We recommend that it be accepted in partial fulfillment of the requirements for the degree of Master of Science in Biology.

_____

Sarah Lundin-Schiller

Committee Chair

_____

Amy Thompson

Committee Member

_____

Gilbert Pitts

Committee Member

Statement of Permission to Use

In presenting this thesis in partial fulfillment of the requirements for the Degree of Master of Science in Biology at Austin Peay State University, I agree that the library shall make it available to borrowers under the rules of the library. Brief quotations from this thesis are allowable without special permission, provided that accurate acknowledgement of the source is made. Permissions for extensive quotation or reproduction of this thesis may be granted by my major professor, or in his/her absence, by the Head of the Interlibrary Services when, in the opinion of either, the proposed use of the material is for scholarly purposes. Any copying or use of the material in this thesis for financial gain shall not be allowed without my written permission.

_____ _____

Justin Lawrence Date

I dedicate this thesis to my father, Jeffrey Lawrence. Without him, none of this would be possible. I love you, Pops.

Acknowledgements

I want to thank my dad, Jeffrey Lawrence, and my stepmother, Anne Lawrence. Your love and support have been more than I could ever ask for. I could not have accomplished anything without you. I also want to thank my committee members, Dr. Gilbert Pitts and Dr. Amy Thompson, for their guidance throughout this entire process. Lastly, I want to thank Dr. Sarah Lundin-Schiller for her understanding, constant reassurance and enormous guidance along the way.

ABSTRACT

The highly metastatic breast cancer cell line, MDA-MB-231, exhibits an altered glycolytic process known as the Warburg effect. The Warburg effect is characterized by increased cellular influx of glucose, use of glycolytic intermediates for anabolic reactions, and preferential conversion of pyruvate into lactate despite presence of oxygen. This suggests that mitochondria have a lessened metabolic role during times of cell growth; however, it is unclear if the Warburg effect is employed during cellular migration as the need for ATP increases for actin filament elongation at a cell's leading edge. Mitochondria have been shown to accumulate in anterior regions of migrating MDA-MB-231 cells aiding in velocity, persistence of migration. Furthermore, MDA-MB-231 cells displaying mitochondria of a fissioned phenotype have increased migration and invasion capabilities. It may be mitochondria are trafficked to anterior regions for supplying ATP via electron transport chain (ETC) for cellular migration. Location and morphology of mitochondria during MDA-MB-231 cell migration via scratch wound assays were compared between non-migratory (NMIG) and migratory cells (MIG), as well as between migratory cells treated with increasing concentrations of epidermal growth factor (EGF; 0 ng/ml, 10 ng/ml, 100 ng/ml). Mitochondrial location was quantified by measuring fluorescence intensity in z stacks of cell images labeled with *MitoTracker* ® Green- FM. To determine if ETC is necessary for cellular migration, migration rates were measured in cells treated with increasing concentrations of sodium azide (NaN_3), a known inhibitor of Complex IV of ETC. Our data showed no redistribution of mitochondria between NMIG cells and MIG cells. In cells treated with EGF there was significant decrease in posterior localization, yet no overall redistribution of mitochondria to a specific location. Furthermore, fissioned mitochondria were the dominant phenotype displayed within all migratory MDA-MB-231 cells and were primarily found in anterior cell regions. The process of migration, yet not EGF treatment, showed an effect upon

mitochondrial phenotype. Migration rates were significantly slowed through inhibition of ETC with 100 mM NaN_3. Although migration does not cause an overall redistribution of mitochondria to anterior regions, the increased presence of fissioned mitochondria in lamellipodia of migratory cells suggests that mitochondria may promote migration by increasing the local supply of ATP through oxidative phosphorylation.

TABLE OF CONTENTS

CHAPTER I: INTRODUCTION

Cell migration is an energy expensive process with lamellipodia dynamics requiring abundant ATP. Mitochondria supply ATP to site-specific areas of high energy needs and reduce ADP:ATP ratios (Cunniff, McKenzie, Heintz, & Howe, 2016; Schuler et al., 2017). Metabolic switches during cell migration have been seen in pancreatic cancer which begs the question of whether MDA-MB-231 metastatic breast cancer cells can do the same (Rozeveld, Schulze, Zhang, & Razidlo, 2019). MDA-MB-231 cells utilize the Warburg effect during times of cell growth but may increase oxidative phosphorylation to provide abundant ATP necessary for cell migration.

An altered metabolism known as the Warburg effect has been studied in many types of cancer as it correlates with cell growth, proliferation, and overall metabolic function of cancer (Han et al., 2013; Matoba et al., 2006; Vander Heiden, Cantley, & Thompson, 2009). Normal cells depend on cellular respiration for efficient ATP synthesis, where glycolysis provides minimal ATP and mainly provides pyruvate and NADH for downstream catabolic processes like the electron transport chain (ETC). In cancer cells, the Warburg effect enhances glycolysis (Robey et al., 2008; Singer et al., 2011), anabolic processes for biomass production (DeBerardinis et al., 2007; Yang, Peng, & Huang, 2018), and preferentially converts pyruvate into lactate despite the availability of oxygen (Fantin, St-Pierre, & Leder, 2006; Shim et al., 1997). This altered metabolism balances anabolic processes and ATP production and it has been proposed that this metabolism is an evolutionary advantage for rapid growth among cancer cells (Liberti & Locasale, 2016; Vander Heiden et al., 2009). With a metabolic focus on generating biomass, the Warburg effect may lessen the need for mitochondrial ATP production in cancer cells, thus allowing enhancement of other processes such as cell migration.

The purpose of this thesis was to determine the mitochondrial location, phenotype and metabolic requirements within migratory MDA-MB-231 cells in scratch wound assays. Utilizing scratch assays and EGF to induce cell migration, mitochondrial location and phenotype was analyzed by z stack imaging and fluorescent staining of nuclei and mitochondria within migratory and non-migratory MDA-MB-231 cells. Sodium azide was utilized to determine the effect of ETC inhibition on migration rates in scratch assays; in addition, a follow-up resazurin assay was performed to assess metabolic activity within cells treated with sodium azide.

Desai, Bhatia, Toner, & Irimia (2013) showed that in migratory MDA-MB-231 cells, mitochondria localized primarily in anterior regions, between the nucleus and lamellipodium, during cellular migration. They utilized mitochondria localization index (MLI) and intensity profiles (IP) to quantify the mitochondria at specific locations. The first goal of this thesis was to determine if cellular migration is associated with a redistribution of mitochondria in MDA-MB-231 cells. To reach this goal the first specific aim was determining if migration caused a redistribution of mitochondria, comparing MLI between non-migratory and migratory cells. Furthermore, previous works have shown that treatment with epidermal growth factor (EGF) increases migration rates in MDA-MB-231 cells (Kim, Kong, Chang, Kim, & Kim, 2016: Bell, Zahn, Grady, & Lundin-Schiller, 2016); thus, the second specific aim was to determine if treatment of increasing concentrations of epidermal growth factor (EGF) affected localization. To identify and quantify mitochondrial location in MDA-MB-231 cells with scratch assays, I utilized the MLI group designation created by Desai et al. (2013); however, instead of utilizing IPs, the z stack imaging method which allows for viewing a three-dimensional objects, was used to quantify mitochondria location among the multiple focal planes of the cell. IPs do not quantify

fluorescence of objects outside of the profile line thus, the use of z stack images will allow for the quantification of mitochondria throughout an entire cell.

Mitochondria are dynamic organelles capable of displaying a fissioned or a fused phenotype. While fissioned mitochondria are able to be trafficked along microtubules, fused mitochondria are unable to be trafficked and are utilized primarily for organelle homeostasis where metabolite transfer between organelles is performed to minimize effects from reactive oxygen species (Caino et al., 2015; Senft & Ronai, 2016). Mitochondrial phenotype has been tied to metastatic potential in breast cancer as highly metastatic cells exhibit fissioned mitochondria and increased migration and invasion capabilities, whereas cells displaying fused mitochondria are less metastatic (Zhao et al., 2013). The second goal of this study was to determine the dominant mitochondrial phenotype in migratory cells, with the first aim being to determine if phenotype differed between non-migratory (NMIG) and migratory (MIG) cells, and the second aim was determining the effect of EGF treatment upon phenotype localization in anterior regions.

MDA-MB-231 cells utilize the Warburg effect for ATP and biomass synthesis during growth and proliferation phases (Yang et al., 2018); although, the new-found importance for mitochondria during cell migration (Desai, Bhatia, Toner, & Irimia, 2013; Zhao et al., 2013) suggests either an increase in oxidative phosphorylation or even a complete switch in metabolism during migratory phases. While metabolic switches have been recently studied in migratory pancreatic cancer (Rozeveld et al., 2019), the importance of mitochondria in MDA-MB-231 cell migration suggests use of mitochondrial metabolism to supply energy for leading edge dynamics; thus a metabolic shift may be occurring. To examine whether migratory MDA-

MB-231 cells depend upon oxidative phosphorylation, our third goal was to determine the effect of ETC inhibition upon cell migration in scratch wound assays.

CHAPTER II: LITERATURE REVIEW

INTRODUCTION

Increased metastatic potential of breast cancer drives poor patient prognoses. Triple negative breast cancer (TNBC) cell line, MDA-MB-231, has been used to study the Warburg effect trademarked by enhanced glycolysis, despite available oxygen for use in oxidative phosphorylation and efficient ATP synthesis (Gatenby & Gillies, 2004; Toschi et al., 2010). However, this altered metabolism enables cells to enhance the ATP produced through glycolysis (Liberti & Locasale, 2016; Vander Heiden et al., 2009), as well as provide more substrates in biomass synthesis necessary for rapid cell growth (Yang et al., 2018). Yet, the Warburg effect decreases utilization of mitochondria for oxidative phosphorylation, due to pyruvate being preferentially converted to lactate (Fantin et al., 2006; Shim et al., 1997). MDA-MB-231 are highly migratory cells and cell migration is an ATP expensive process, where actin filaments in leading edges of migratory cells require abundant ATP to elongate and extend the lamellipodia as the cell moves forward. The anterior location and fissioned phenotype of mitochondria increase migration and invasion of MDA-MB-231 cells (Desai et al., 2013; Zhao et al., 2013). This suggests that these cells traffic mitochondria to anterior regions for ATP supplement necessary for actin elongation. More importantly, it suggests MDA-MB-231 cells may be capable of switching the primary metabolism depending on a cellular need to grow versus migrate.

It has been shown that MDA-MB-231 cells utilize the Warburg effect to drive growth through anabolic processes (Fantin et al., 2006; Liberti & Locasale, 2016; Shim et al., 1997), and other studies show that mitochondria are important for cell migration and invasion (Desai et al., 2013; Zhao et al., 2013). However, the literature does not adequately describe the metabolic

dynamics of MDA-MB-231 cells in response to cell migration. This review will first highlight breast cancer and the MDA-MB-231 cell line phenotype, making it an important cell line to study. I will then present an overview of the Warburg effect, examining how this altered metabolism increases anabolism for cell growth. Next, cellular migration mechanics and cancer metastasis will be reviewed. Lastly, I will cover how mitochondria may be more beneficial for cellular migration by providing local ATP through catabolic processes.

BREAST CANCER AND MDA-MB-231

Breast cancer is the second leading cause of cancer deaths in women, affecting 1 in 8 women in their lifetime. Metastatic potential of certain breast cancers drives poor prognoses in patients. The American Society of Clinical Oncology (ASCO) reports that 5 year-survival rates drop from 99% to 85% if the cancer has spread to a regional lymph node, and as low as 27% if metastases are found in distant parts of the body (Cancer.net, 2019). There are at least 84 different breast cancer cell lines, each of which expresses differing tumorigenic aberrancies (Dai et al., 2017).

The invasive ductal breast carcinoma cell line MDA-MB-231 is highly metastatic, partly due to a rapid migratory phenotype and partly due to this cell line's ability to double the number of cells every 24 hours. MDA-MB-231 cells are used to study the phenomenon known as the Warburg effect and may be the culprit behind the 24-hour doubling rate. Most breast cancers have one of three main hormone receptors used by the cells to fuel growth and proliferation: estrogen receptor (ER), progesterone receptor (PR), and human epidermal growth factor receptor 2 (HER2). These common receptors are used as targets for hormone therapy and other pharmacological treatments. For example, the selective estrogen receptor modulators (SERMs)

tamoxifen and raloxifene are commonly used to treat breast cancers positive for ER (Cancer.org, n.d.). They both act as estrogen antagonists by blocking estrogen receptors in breast tissue yet tamoxifen can also act as an estrogen receptor agonist in other tissues such as the uterus (Nazarali, Narod, & Narod, 2014). For cancers with HER2 receptors, the use of antibodies trastuzumab combined with pertuzumab can inhibit these growth receptors.

However, the MDA-MB-231 cell line is known as a triple negative breast cancer (TNBC). Being a TNBC line means that they lack the three main receptors: ER, PR, and HER2. Without these receptors to target, hormone therapy becomes an unreliable treatment against TNBC cells, and less selective treatments like chemotherapy would need to be employed. Yet, there is a receptor which MDA-MB-231 cells highly expresses: epidermal growth factor receptor (EGFR). The presence of EGFR allows for the use of epidermal growth factor (EGF) as a chemoattractant for the study of the rapid migratory phenotype. Bell et al. (2017) found that MDA-MB-231 cell migration increases with the treatment of EGF. Thus, use of EGF will enable one to study the mechanical and metabolic nature behind MDA-MB-231 cell migration.

THE WARBURG EFFECT

First observed by Otto Warburg (1956), proliferating cancer cells had altered their metabolism to convert glucose into lactate despite the availability of oxygen in the environment. The switch from the efficient ATP production pathways of electron transport chain (ETC) and oxidative phosphorylation, to a less efficient glycolytic pathway could be a byproduct of nutrient availability and pressure for the cancer cells to grow and divide rapidly.

When unicellular organisms are surrounded by an abundance of nutrients, the evolutionary pressure is to grow and divide until the nutrients run scarce; however, control systems are in place that sense nutrient availability and channel metabolic processes to generate building blocks for division (Vander Heiden et al., 2009). For multicellular organisms, cooperation and coordination between all cells is required for the survival of the organism as a whole. In human tissues, the supply of glucose and other nutrients is abundant and thus control systems within each cell prevent aberrant proliferation when nutrient supply exceeds what is necessary for division (Vander Heiden et al., 2009). Due to genetic instability and downstream dysregulation of those control systems, cancer cells are able to and use these abundant nutrients and proliferate uncontrollably (DeBerardinis et al., 2007; Zhang, Zhao, Tong, & Guan, 2015). These proliferative cancer cells can have an increased glucose intake, up to 100 times the normal rate due to the Warburg effect (Alberts et al., 2015).

During normal aerobic cell metabolism, ATP synthesis occurs through the major catabolic pathways of glycolysis, Kreb's cycle, and the ETC. Glycolysis provides two ATP per glucose molecule, and oxidative phosphorylation and ETC provide 34 ATP per glucose, making oxidative phosphorylation a more efficient process for ATP synthesis. However, glycolysis can also be used in anaerobic environments, where oxidative phosphorylation cannot occur. In this condition, each glucose molecule is broken down into two pyruvates and each pyruvate is converted into lactate via lactate dehydrogenase (LDH). LDH converts pyruvate into lactate through oxidation of NADH to NAD^+. Lactate is then shuttled out of the cell and the oxidized NAD^+ can be recycled for another round of glycolysis (Liberti & Locasale, 2016).

The Warburg effect displays preferential fermentation of pyruvate into lactate despite the availability of oxygen (Fantin et al., 2006; Shim et al., 1997). Additionally, the Warburg effect is

also characterized by an increased glucose influx into the cell (Adekola, Rosen, & Shanmugam, 2012; Singer et al., 2011; Zhang et al., 2015). Heightened glucose import, and decreased use of catabolism through oxidative phosphorylation, is suggested to enable the use of glycolytic intermediates for anabolic reactions required for rapid cell growth and proliferation The intermediate of glycolysis, glucose-6-phosphate, can be used in the anabolic process of pentose phosphate pathway (PPP) to convert $NADP^+$ into NADPH and create ribose-5-phosphate needed for nucleotide synthesis (Jin & Zhou, 2019). Recently, it has been shown that the key enzyme in linking glycolysis to PPP, 6-phosphogluconate dehydrogenase (6GPD), has heightened protein expression in MDA-MB-231 cells where knockdown of 6GPD arrests cell growth significantly more in MDA-MB-231 cells than in normal cells (Yang et al., 2018). Another glycolytic intermediate, glyceraldehyde-3-phosphate, can be used in a secondary anabolic pathway where a conversion into glycerol-3-phosphate is used for lipid synthesis (DeBerardinis et al., 2007). Therefore, the elevated glycolysis displayed by the Warburg effect is believed to allow for these glycolysis intermediates to be utilized in the production nucleotides and lipids necessary for rapid growth and proliferation (DeBerardinis et al., 2007; Liberti & Locasale, 2016; Vander Heiden et al., 2009), possibly increasing tumor growth and extracellular acidification through increased lactate export.

This altered metabolism may be an evolutionary adaptation to supply cells with building blocks for rapid growth and proliferation. Yet, one can imagine that as a tumor grows and cells are densely packed within, so too does competition among those tumor cells. Some cells may need to migrate out to acquire nutrients elsewhere thus, metastasis begins as cells utilize the ATP-expensive process of migration to seek out receptive tissues and inhabit distant parts of the body.

CANCER METASTASIS

MDA-MB-231 cells are commonly used as a model for the study of metastasis due to their aggressive migratory behavior (Desai et al., 2013; Poincloux et al., 2011; Smelser et al., 2015; Zhao et al., 2013). Metastasis involves four stages: intravasation, survival in circulatory system, extravasation, and establishment of secondary tumors (Krakhmal et al., 2015). While tumor cells continuously grow and proliferate, some begin an epithelial to mesenchymal transition (EMT) once a reduction of E-cadherin adhesion molecules occurs (Krakhmal et al., 2015). Losing these adhesion molecules allows the cells to adopt a migratory phenotype, break away from the tumor and migrate into the circulatory system (intravasation). Cells travel the circulatory system and eventually into tight capillaries where they will exit the capillary and migrate into the surrounding tissues (extravasation). Once in the tissue the cell re-expresses cadherin adhesion molecules, losing the migratory phenotype through mesenchymal to epithelial transition (MET), as the cell begins to grow and divide to set up a secondary tumor.

But, how does a migrating cancer cell "know" where to go? It has been long known that certain cancers metastasize to specific areas. This concept is known as the "seed and soil" hypothesis, first mentioned by Stephen Paget (1889). Cancer cells (seed) metastasize throughout the body but will succeed in setting up tumors only in receptive areas (soil). Each seed has unique soils that are receptive for further growth. For example, breast cancer is known to metastasize to bone tissue (Langley & Fidler, 2011). This is suggested to be caused by growth factors such as chemokines that bone tissue expresses which act as homing beacons for metastasizing cells (Ibrahim et al., 2000, Guise 2010).

CELLULAR MIGRATION

Cellular migration is a highly conserved process among many unicellular and multicellular organisms, as cells sometimes need to move to access nutrients or environments where they can thrive. In multicellular organisms, cells can exhibit different migratory behaviors (Vicente-Manzanares, 2005). For example, fish keratocytes are able to migrate as single cells with broad fan-like leading edges (Okimura, Taniguchi, Nonaka, & Iwadate, 2018), human epithelial cells can migrate as interconnected sheets of tissue during gastrulation and wound healing or as single cells with fibroblast-like migration (Kurosaka & Kashina, 2008), and macrophages can display amoeboid movement via extension of pseudopodia (Rosania & Swanson, 1996). MDA-MB-231 cells display a fibroblast-like morphology and aggressive migratory behavior.

Fibroblast migration is achieved through actin filament reorganization, where extending actin filaments create a leading cell edge, or lamellipodia, that protrudes in the direction of migration. Leading edge protrusion allows adhesion molecules to attach to the substrate while at the same time the cell's trailing edge retracts as adhesion molecules detach from the substrate to propel the cell forward (Vicente-Manzanares, 2005). Migration requires cooperation between different biomechanical processes. Extension of actin filaments is dependent upon abundant cytosolic ATP, as the molecule is hydrolyzed to bind monomeric G-actin together, creating filamentous F-actin (Korn et al., 1987). Simultaneously, myosin filaments at the rear of the cell generate contractile forces resulting in the release of rear adhesion molecules (Chi et al., 2014; Poincloux et al., 2011). Cooperation between the actin extension and myosin-mediated contraction enables polarization of the cell as it begins to migrate forward.

ROLE OF MITOCHONDRIA IN CELLULAR MIGRATION

Mitochondria are the site of Kreb's cycle and oxidative phosphorylation used in the catabolic breakdown of glucose for ATP synthesis. Pyruvates from glycolysis are transported into the mitochondrial matrix and broken down further in the Kreb's cycle producing substrates for oxidative phosphorylation where the ETC and chemiosmosis are utilized to produce ATP. Mitochondria are also dynamic organelles that can undergo fusion and fission (Chen & Chan, 2017). Regulation of these phenotypes is dependent upon cell stress and homeostasis, or need for mitophagy and dispersal of the organelles during cell division (Farmer et al., 2018); thus fusion and fission are equally important as the coordination between the two is essential for overall cell survival. Mitochondrial dynamics also have an impact upon migration and invasion of breast cancer (Zhao et al., 2013), where dispersal of mitochondria to leading edges (Desai et al., 2013) may provide local supply of ATP to actin networks of lamellipodia.

Mitochondrial fusion allows for these organelles to form into long tubular networks. Fusion between two or more organelles is a process of first combining the outer mitochondrial membrane (OMM) followed by the fusion of the inner mitochondrial membrane (IMM). The fusion of these membranes is regulated by different proteins. Mitofusion 1 and 2 (Mfn1 and Mfn2) fuses the OMM and Optic Atrophy 1 (OPA1) fuses the IMM (MacVicar & Langer, 2016). Although Mfn1 and Mfn2 can be used interchangeably to fuse the OMM (Chen et al., 2003), OPA1-mediated fusion of the IMM is dependent upon Mfn1 (Cipolat, De Brito, Dal Zilio, & Scorrano, 2004). Fusion is utilized to transfer mitochondrial metabolites between fused organelles for organelle homeostasis, as well as possibly maintaining cell survival during times of stress by increasing ATP synthesis (Farmer et al., 2018; Chen et al., 2005; Silva Ramos et al., 2016).

In contrast to extensive tubular networks of fused mitochondria, fissioned mitochondria are smaller, thus able to be trafficked throughout the cell. A key protein long known to be involved in mitochondrial fission is dynamin-related protein 1 (Drp1) (Smirnova, Griparic, Shurland, & Van der Bliek, 2001), however there are other factors that allow the fission process to occur. Initiation of fission is started by the endoplasmic reticulum which constricts fused mitochondria (Friedman et al., 2011), followed by the recruitment of Drp1 to receptors on mitochondrial membrane to further the constriction (Losó n, Song, Chen, & Chan, 2013). However, Drp1 recruitment is not enough to completely fission the organelle as the associated protein dynamin-2 (Dyn2) is necessary to pinch the fused structure into two separate organelles (Lee, Westrate, Wu, Page, & Voeltz, 2016). Fission allows for the appropriation of roughly equal organelles to daughter cells after cell division (Pagliuso, Cossart, & Stavru, 2018), as well as produces organelles capable of mitophagy and controlling the overturn of new mitochondria (Narendra, Tanaka, Suen, & Youle, 2009). Furthermore, the ability to be trafficked along microtubule "highways" gives the cell the opportunity to provide a local supply of ATP to alleviate high ADP:ATP ratios (Cunniff et al., 2016; Schuler et al., 2017). MDA-MB-231 cell line has been associated with higher levels of Drp1 than the lesser metastatic cell line MCF7 which has higher levels of Mfn1 (Zhao et al., 2013). Indeed, Zhao et al. (2013) displayed how the knockdown of Drp1 through siRNA interference led to significant decrease in the migration and invasion capabilities of MDA-MB-231 cells. Increased migration may be due to the ability of fissioned mitochondria to be trafficked to areas of high energetic needs. Trafficking mitochondria involves mitochondrial RhoGTPase 1 (miro1) which links the organelle to microtubules for dispersal throughout the cell. It has been shown that cells can strategically traffic mitochondria to areas of high ADP:ATP ratios to supply a local source of ATP (Schuler et

al., 2017). Other areas of high energetic need are the actin networks along lamellipodia of migratory cells, where actin requires ATP hydrolysis for elongation (Korn et al., 1987). Anterior localization of mitochondria has been seen to aid in velocity and persistence in MDA-MB-231 cell migration (Desai et al., 2013); thus it is suggested that mitochondria in lamellipodia are necessary for providing a local source of ATP required in actin elongation. This suggestion confronts the notion that MDA-MB-231 cells' utilization of the Warburg effect decreases the use of mitochondria for oxidative phosphorylation. However, it does provide a scenario that MDA-MB-231 cells may switch the primary metabolism to oxidative phosphorylation after migration is induced.

LITERATURE REVIEW SUMMARY

MDA-MB-231 cell line has been used in studies of cell growth and cell migration which utilize seemingly opposing metabolisms. The altered metabolism seen in MDA-MB-231 cells is characterized by increased lactate production (Warburg, Otto 1956), increased glucose import (Adekola et al., 2012; Singer et al., 2011), and preferential conversion of pyruvate into lactate despite the availability of oxygen (Shim et al., 1997). This metabolism is suggested to provide glycolysis intermediates for the anabolic production of nucleic acids and lipids to fuel cell growth and proliferation (Vander Heiden et al., 2009). With a preferential conversion of pyruvate into lactate, there is a decrease in oxidative phosphorylation (Fantin et al., 2006) suggestive of a decreased need for mitochondria within these cells.

Mitochondria are dynamic organelles capable of fusion and fission between other mitochondria. Fusion allows for the transfer of metabolites and other materials to maintain

organelle homeostasis and mtDNA (Chen et al., 2005; Farmer et al., 2018; Silva Ramos et al., 2016). In contrast, fissioned mitochondria are used for trafficking organelles to intracellular areas with high energy needs (Cunniff et al., 2016; Schuler et al., 2017). During cellular migration, lamellipodia protrusion is mediated by the elongation of actin networks. Actin requires abundant ATP as extension of filaments is achieved by ATP hydrolysis (Korn et al., 1987), thus fissioned mitochondria may be trafficked to supply elongating actin with a local supply of ATP for cellular migration. Indeed, a recent study has shown fissioned mitochondria being predominantly displayed within highly metastatic cell line MDA-MB-231, relating to increased migration and invasion when compared to a lesser metastatic cell line, MCF7, that displays fused tubular networks (Zhao et al., 2013). Furthermore, Desai et al. (2013) showed mitochondria localizing in anterior regions of migratory MDA-MB-231 cells, causing increased velocity and persistence of migration.

The literature reveals a gap where studies tend to cover the Warburg effect upon cell growth, or migration within the MDA-MB-231 cell. The metabolisms involved seem to oppose each other and are not discussed as possible dynamic processes which the cell may switch depending upon the pressure to grow versus migrate. This thesis will expand upon existing literature describing mitochondrial dynamics in MDA-MB-231 cell migration, to determine if cells are dependent upon oxidative phosphorylation for cellular migration.

CHAPTER III: MATERIALS AND METHODS

CELL CULTURE

MDA-MB-231 cells were purchased through American Type Culture Collection (ATCC catalog #HTB-26). Cells were grown in Modified Eagle's Medium, MEM, (Gibco, catalog # 11095-080) supplemented with 10% fetal bovine serum (FBS) (Gibco, catalog # 26140-087), 2% Antibiotic/Antimycotic (Ab/Am) (Gibco, catalog # 15240-096) and incubated at 37 °C in an atmosphere of 5% CO_2 in air. Half of the media was replaced every 2-3 days.

SUBCULTURING

All media was removed from seed flask, and 5 mL of Trypsin-EDTA 1X (Gibco, catalog # 15400054) was added to the flask and incubated for 10 minutes to release the cells adhering to the flask. Cell-trypsin mixture was added to 3 mL of growth media and centrifuged at 125 x g to form a cell pellet. Supernatant was decanted, 5 mL of growth media added to pellet, and mixture was vortexed to resuspend the cells in the media. 1 mL of cell mixture was added to 4 mL fresh media in a new seed flask for reseeding at a 1:5 ratio. Subculturing was performed every 7 days.

NUCLEAR AND MITOCHONDRIAL STAINING

Cultured cells were plated in 35 mm glass bottomed dishes (Ibidi No. 1.5 coverslips, catalog #81218-200) and grown to confluence over 48 hours. Cells were stained with 100 nM MitoTracker Green FM (MTG) (Invitrogen, catalog # M7514) for mitochondrial visualization, and 3 mg/50 ml Hoechst 33342 (Sigma, product # B2261) for nuclear visualization. Staining was

performed by adding a cocktail of 1 mL Hoechst mixed with 0.2 mL MTG and 0.8 mL MEM and incubating for one hour. The cocktail was then removed, and cells were rinsed twice with 1X PBS to remove staining cocktail. A scratch was then made with a 200 µL pipet tip (Eppendorf epT.I.P.S., catalog # 22492039) through the confluent monolayer creating a wound 1.5-2 mm wide. Cell debris was washed with 1X PBS before adding 1 mL Phenol (-) MEM (Gibco, catalog # 51200-038) supplemented with 10% FBS and 2% Ab/Am to cells for imaging

NORMALIZATION OF NUCLEI AND MITOCHONDRIAL LOCATION ANALYSIS

Nuclear position within the cell is crucial to determining localization of mitochondria. To lessen bias in the mitochondrial measurements, nuclear positioning was calculated. Anterior and posterior regions were determined in migratory cells by the direction of migration. Anterior and posterior regions in non-migratory cells were determined by where a cell was relative to the scratch, with anterior being closer and posterior being farther away from the direction of the scratch. Using the following equation: $((C - M) / L)$, determining a cell's nuclear position began by measuring the distance between the posterior and anterior boundaries of the cell (denoted as L). Half of the length of the cell was determined to be the midpoint (M). Distance was then measured from the posterior boundary to the centroid of the nucleus (C). The difference between the centroid and midpoint ($C - M$) was then divided by L. A positive normalization indicated the nucleus was "leading" in front of the midpoint, whereas a negative normalization was indicative of a "lagging" nucleus.

To determine the location of mitochondria within migrating MDA-MB-231 breast cancer cells, the method performed by Desai et al. (2013) was used with modifications. Use of Intensity

profiles for analysis may not account for the three-dimensional nature of cells; instead z stack imaging was used to quantify organelle location throughout the entire cell. Figure 1 exhibits how an intensity profile line measured fluorescence within a migratory cell.

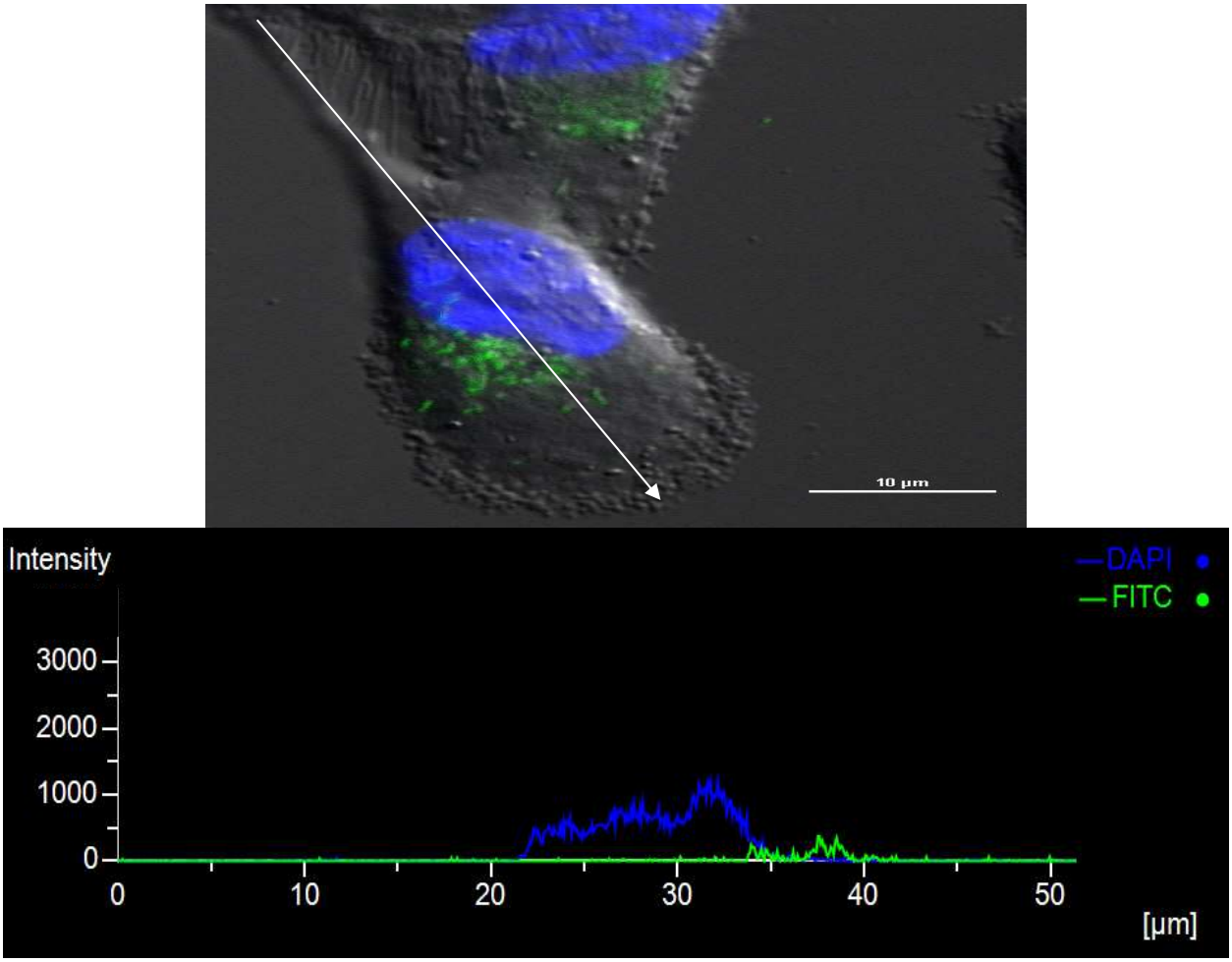

Figure 1. (Above) Migratory cell used for intensity profile line scan (white line). Line scan begins at trailing edge of cell and extends to leading edge. (Below) An intensity profile was used to determine localization of green fluorescent mitochondria (FITC) relative to location of blue fluorescent nucleus (DAPI) along length of the profile line scan. Length of cell, shown in micrometers, is on the X-axis. Fluorescence intensity from DAPI and FITC channels is on the Y-axis. This profile shows that mitochondria (green line) were localized anterior to the nucleus (blue line) but the line scan ignored fluorescent intensity values of objects outside of the profile line.

In order to quantify localization of all mitochondria throughout a three-dimensional cell, a z stack image method was instead utilized in this thesis. Four (4) random fields of view were studied using confocal microscopy. Migrating cells were viewed along the cell fronts of the scratch assay as cells migrated inward towards the gap establishing a direction of migration that enabled assignment of anterior and posterior cell regions. Non-migrating cells were viewed away from the scratch. To define anterior and posterior regions of non-migrating cells, the half of the cell which was closest to the direction of the scratch was defined as anterior, and the opposite cell half defined as posterior. Each field of view was analyzed using NIS Elements software (Nikon Instruments, Inc.) to create Z stack maximum intensity images to visualize all mitochondria among the multiple focal planes of the cells. Mitochondrial fluorescence was calculated by using the centroid of the nucleus to split the cell into two primary regions of interest (ROI), an anterior and reciprocal posterior region. The mitochondrial intensity levels were quantified within each primary ROI through thresholding mitochondria within secondary ROIs using NIS elements. Thresholding identifies all fluorescent objects through DAPI and FITC filters and places an ROI around these objects to quantify the objects' intensity levels. In this way, all mitochondria within primary ROIs were accounted for. Figure 2 exhibits the establishment of primary and secondary ROIs on an image of a migratory cell.

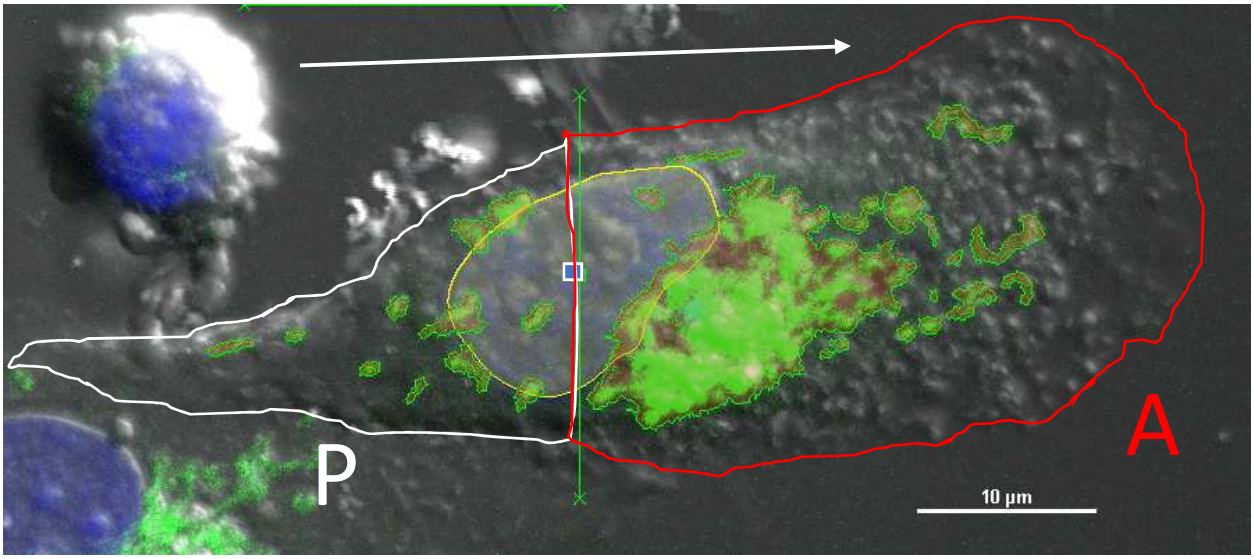

Figure 2. Fluorescent confocal image exhibiting primary and secondary ROI on a migratory MDA-MB-231 cell, where direction of migration is defined by white arrow lines. To measure mitochondrial localization an ROI was drawn around entirety of the cell. Direction of migration (white arrow line) and centroid of nucleus (white square) were used to split the ROI into two primary ROIs: anterior (red outline) and posterior (white outline), separated by a line through the centroid (green line through white square). Green fluorescent mitochondria were marked as secondary ROI (objects with green border) to measure intensity levels of all secondary ROIs within each primary ROI (Anterior and Posterior).

The mitochondrial localization index (MLI) was assessed by dividing the sum of the anterior FITC intensity values by the sum of both anterior and posterior FITC intensity values, as shown in the following formula:

$$\frac{\Sigma(A)}{\Sigma(A+P)}$$

MLI values fell within a range of 0 to 1. Values from 0 – 0.35 were marked as posterior localizations, from 0.35 – 0.70 were peri-nuclear localizations, and those from 0.70 – 1 were anterior localizations.

EPIDERMAL GROWTH FACTOR (EGF) TREATMENT

EGF was used as a chemoattractant to increase migration rates in MDA-MB-231 cells. A stock solution of EGF was created by adding EGF (100 µg, Gibco, catalog #PHG0313) to 990 mL of a 15% solution of trehalose in PBS. The stock solution was then separated into 10 µL aliquots and stored at -20°C until needed. When required, the stock solution aliquot was thawed and diluted further into 9990 µL of phenol-free MEM, resulting in a new solution of 100 ng/mL. A 1:10 dilution of the EGF stock solution was also used in this study (10 ng/ml).

MITOCHONDRIAL PHENOTYPE ASSESSMENT

Z stack maximum intensity projection images from the mitochondrial localization studies were re-analyzed to determine the mitochondrial phenotype displayed between non-migratory cells and migratory cells, as well as between cells treated with increasing concentrations of EGF (0, 10, and 100 ng/ml). Mitochondria were qualitatively labelled linked (L) if cells displayed fused networks, and Fissioned (F) if displaying fragmented organelles. Location of fissioned mitochondria in the anterior region was further noted as yes (Y) or no (N). Determination of morphology was obvious for most samples, but for samples with mitochondria that are tightly clumped together the image was further visualized with volume view and slice view image techniques through the NIS Elements software. Volume view and slice view enabled visualization of the cell as a three-dimensional object which allowed for better viewing of the side of the cell where clumps of mitochondria would appear as more spread out, thus easier to determine morphology.

EFFECT OF SODIUM AZIDE ON MDA-MB-231 MIGRATION RATES

Sodium azide (NaN_3) (Sigma, catalog #26628-22-8) was dissolved in MEM growth media to create a stock concentration of 100 mM. An original dilution of 1:5 was used for cells treated with 20 mM NaN_3, a further 1:2 dilution used for cells treated with 10 mM, and a 1:10 serial dilution used for treatments of 1.0, 0.1, 0.01, 0.001 mM working concentrations. For assays examining the effect of 0.001-20 mM NaN_3 upon migration, cells were plated in 12-well plates at a concentration of 80,000 cells/mL (Table 1, 2) and incubated for 2-3 days in 37°C with 5% CO_2 in air until a confluent monolayer formed. Assays examining 0.001-10mM NaN_3 were performed on four 12-well plates with two treatment replications per plate (Table 1). Assays incorporating 20 mM utilized two 12-well plates with two replications per treatment (Table 2). Later assays included 100 mM and excluded 0.001 mM due to no effect seen at that time and not enough room in the plate to uphold equal replication between all treatments. In these assays, 0.5 mL of medium containing 40,000 cells/mL were plated in four replications in two 24-well plates (Table 3).

A P-200 pipette tip was used to create a scratch line with an average width ranging from 1.5-2 mm. Cell debris was washed twice with 1X PBS and MEM supplemented with 10% FBS and 2% Ab/Am was added with treatment. The control well only received MEM growth media. Scratch gap width was measured in micrometers (μm) at Time = 0 hr. The plates were then incubated at 37°C with 5% CO_2 in air for 6 hours and a second gap measurement was taken at Time = 6 hr. The difference in gap width (Δ Gap distance (μm)) between times 0 hr. and 6 hr. was calculated. The difference was divided by 6 hours to find the rate at which the scratch gap closes, which is equivalent to the rate migration of the cells (Δ Gap distance (μm/hr.)).

Table 1. 12-well set up for cells given treatments of NaN_3 concentrations of 0-10mM.			
0	0.001	0.01	0.1
1	10	10	1
0	0.001	0.01	0.1

Table 2. 12-well set up for cells given treatments of NaN_3 concentrations of 0-20mM.			
0	0.01	0.1	1
10	20	20	10
0	0.01	0.1	1

Table 3. 24-well set up for cells given treatments of NaN_3 concentrations of 0-100mM.					
0	100	10	1	0.1	0.01
0	100	10	1	0.1	0.01
0	100	10	1	0.1	0.01
0	100	10	1	0.1	0.01

TRYPAN BLUE EXCLUSION ASSAY

Following the sodium azide migration assay, MEM and treatment were removed from each well and 1mL of 0.4% Trypan Blue (Sigma, catalog #72-57-1) was added to stain for dead cells. Trypan staining was allowed for 15 minutes and then removed and replaced with 1mL HBSS for observation and cell counting. For control and each treatment, three (3) random fields of view were imaged at 100X total magnification with phase contrast microscopy. All cells were counted and dead cells which took up the Trypan Blue were reported. Cell viability of greater than 90% was determined to be acceptable. % Cell viability was quantified by the following equation:

$$\frac{\#\ of Cells\ Not\ Stained}{Total\ \#\ of\ Cells}\ X\ 100$$

RESAZURIN ASSAY FOR METABOLIC ACTIVITY

A resazurin stock solution (2.2 mg/10 mL, 440μM) (Allied Chemicals) was first prepared in PBS and sterile filtered through 0.22 um syringe filter. A NaN_3 stock solution (650 mg/10 mL, 1 M) (Sigma, catalog #26628-22-8) was prepared in PBS and sterile filtered through 0.22 um syringe filter. Final working concentrations were created through 1:10 serial dilutions. Cells were plated in a 24-well plate at an original concentration of 40,000 cells/mL without fetal bovine serum and left to incubate for 24 hours at 37°C with 5% CO_2 in air until they became approximately 75% confluent. Media was removed from all wells and the cells were rinsed once with phenol-free and FBS-free growth media. NaN_3 was given to cells in increasing concentration (0.1, 1, 10, and 100 mM). Control wells were only given phenol-free and FBS-free

media. Total volume in each well, including wells used for blanks (no cells added), was 500 µL. Each treatment was tested in quadruplicate (Table 4). Cells were incubated for a total of 30 minutes. After treatment, NaN_3 was left in the wells and 50 µL of 440 µM resazurin solution was added to each well for a final volume is 550 µL and final resazurin concentration of 44 µM. The breakdown of resazurin (blue, nonfluorescent) into resorufin (pink, fluorescent) via mitochondrial metabolic activity was analyzed with a BioTek Synergy HT plate reader (Biotek Instruments Inc., Winooski, Vermont). Fluorescence of resorufin was viewed using UV light at 540 nm excitation and 590 nm emission. Quantification of resorufin fluorescence was measured using a plate reader every 30 minutes from time 0-4 hours. After which, the plate was incubated over-night and another measurement was taken at time 16.75hr.

Table 4. 24-well treatment layout for resazurin assay protocol. All wells, not including Blanks, were seeded at original cell concentration of 40,000 cells/mL and incubated until reaching ~75% confluency before addition of treatments.

Blanks	Controls (mM)	Treatments Na Azide (mM)			
No Cells	0	0.1	1	10	100
No Cells	0	0.1	1	10	100
No Cells	0	0.1	1	10	100
No Cells	0	0.1	1	10	100

STATISTICAL ANALYSIS

For nuclear positioning ANOVA was utilized to compare across non-migratory and migratory cells with and without EGF treatment. In determination of mitochondrial location among migratory and non-migratory cells, contingency analysis determined observed vs. expected mitochondrial distributions, and Student's t-test was used for the analyses of average total MLI and average anterior MLI. Within EGF treated cells (0ng/ml, 10ng/ml, and 100ng/ml), ANOVA was used to analyze average total MLI. Post-hoc Dunnett's test was used to determine significance among treatments to Control (0ng/ml). Mitochondrial phenotype was analyzed qualitatively to determine linked (L) and fissioned (F), as well as if the phenotypes are located within lamellipodia, yes (Y) or no (N). Percentages of cells with fissioned mitochondria in lamellipodia were then compared across treatments by contingency analysis. To test the effect of increasing concentrations of sodium azide (0mM-100mM) upon cellular migration, groups were analyzed using one-way and two-way ANOVA, with post-hoc Tukey-Kramer HSD to test between all groups and Dunnett's test to compare treatment groups to Control (0mM). Where significant difference in sample variance occurs, Welch's ANOVA was used in place of ANOVA. Repeated Measures ANOVA was used to compare the interaction between time and treatment upon relative fluorescent units (RFU) of resorufin fluorescence. Slopes of each treatment were further compared to control (0 mM) with post-hoc Dunnett's test. Difference between all groups were also compared with post-hoc Tukey-Kramer HSD. All statistical analyses were performed using JMP Pro 14 software (JMP, SAS Institute, Inc., Cary, NC) or Microsoft Excel (Microsoft, Redmond, WA). $P \leq 0.05$ was considered statistically significant.

CHAPTER IV: RESULTS

MITOCHONDRIAL LOCALIZATION WITHIN MDA-MB-231

Quantification of Nuclear Position

The position of the nucleus is critical in determining the localization of mitochondria within migrating cells. To verify that the nucleus was not taking up most of the cytosolic area and prohibiting the trafficking of mitochondria, the nuclear position (NP) within migratory and non-migratory MDA-MB-231 cells was calculated. As shown in Figure 3 *L* was at 75.48 μm, where *M* would be half of total length (37.74 μm), and *C* was at 44.41 μm. Taking the normalization equation ((*C* – *M*) / *L*), the position of the nucleus was 0.088, representing a slightly "leading" nucleus.

Figure 4 shows the average NP within non-migratory (n=59) and migratory cells with increasing concentrations of EGF (0 ng/ml EGF n= 38, 10 ng/ml EGF n=67, 100 ng/ml n=65). NPs for each cell were analyzed to make sure nuclear positioning did not bias the localization of mitochondria within the cells towards a more anterior or posterior position. The NP was not significantly altered by migratory status nor EGF treatment (0, 10, and 100 ng/ml EGF) (ANOVA, $p > 0.05$).

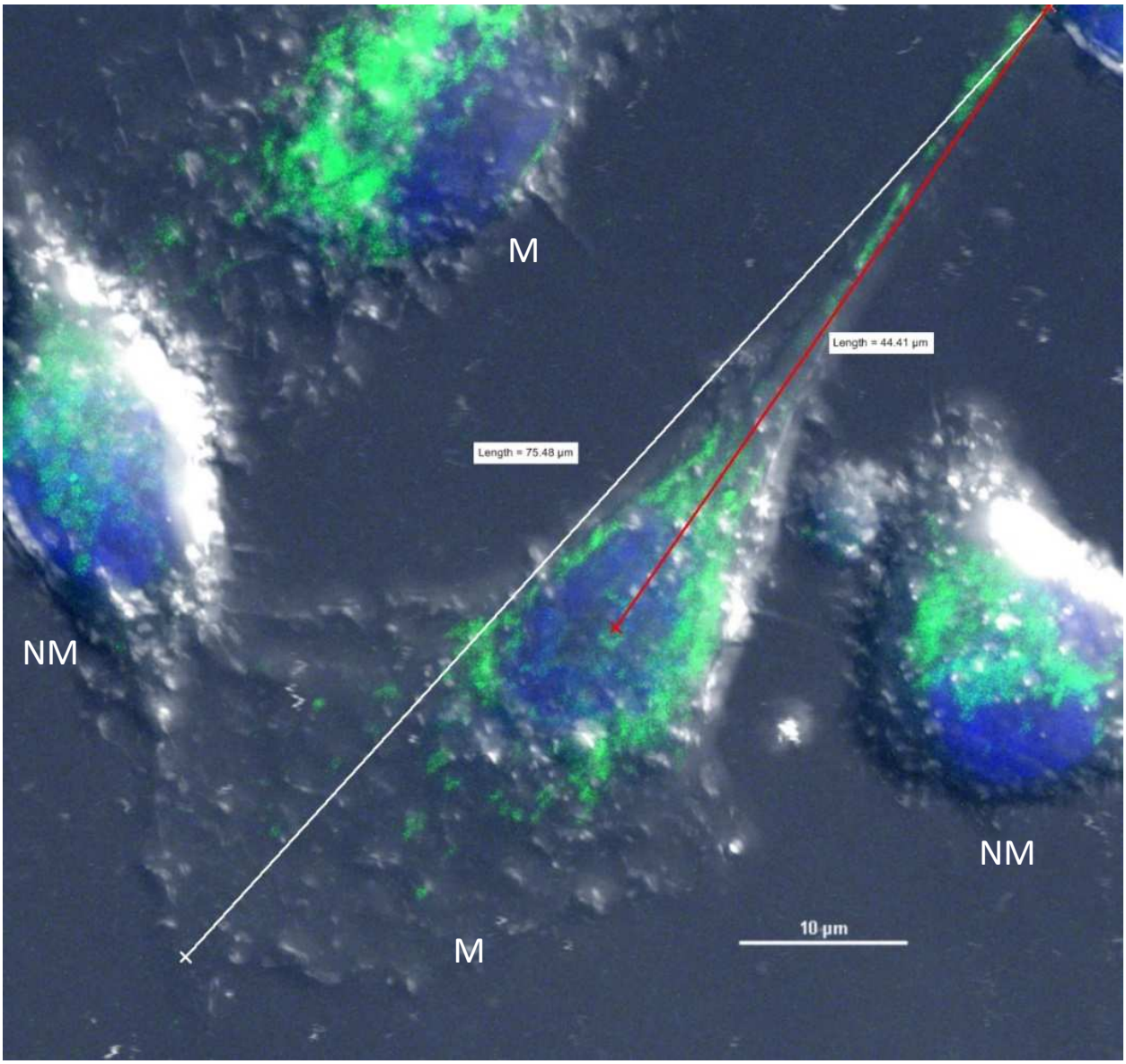

Figure 3. Z-Stack image of migratory (white M) and non-migratory (white NM) MDA-MB-231 cells, nuclei (blue) and mitochondria (green). Extended lamellipodium during migration was used to locate nuclear position (NP) within the migratory cell. Full length of cell (L; white line = 75.48 µm), and distance from nuclear centroid to rear (C; red line = 44.41 µm) were measured. Midpoint (M) was calculated by dividing length by two (M = L/2). NP was calculated using the formula (C-M)/L. NP of this migratory cell was (44.41-37.74)/75.48 = 0.09. Positive values indicate the nucleus is "leading" past the midpoint, negative values indicate a "lagging" nucleus.

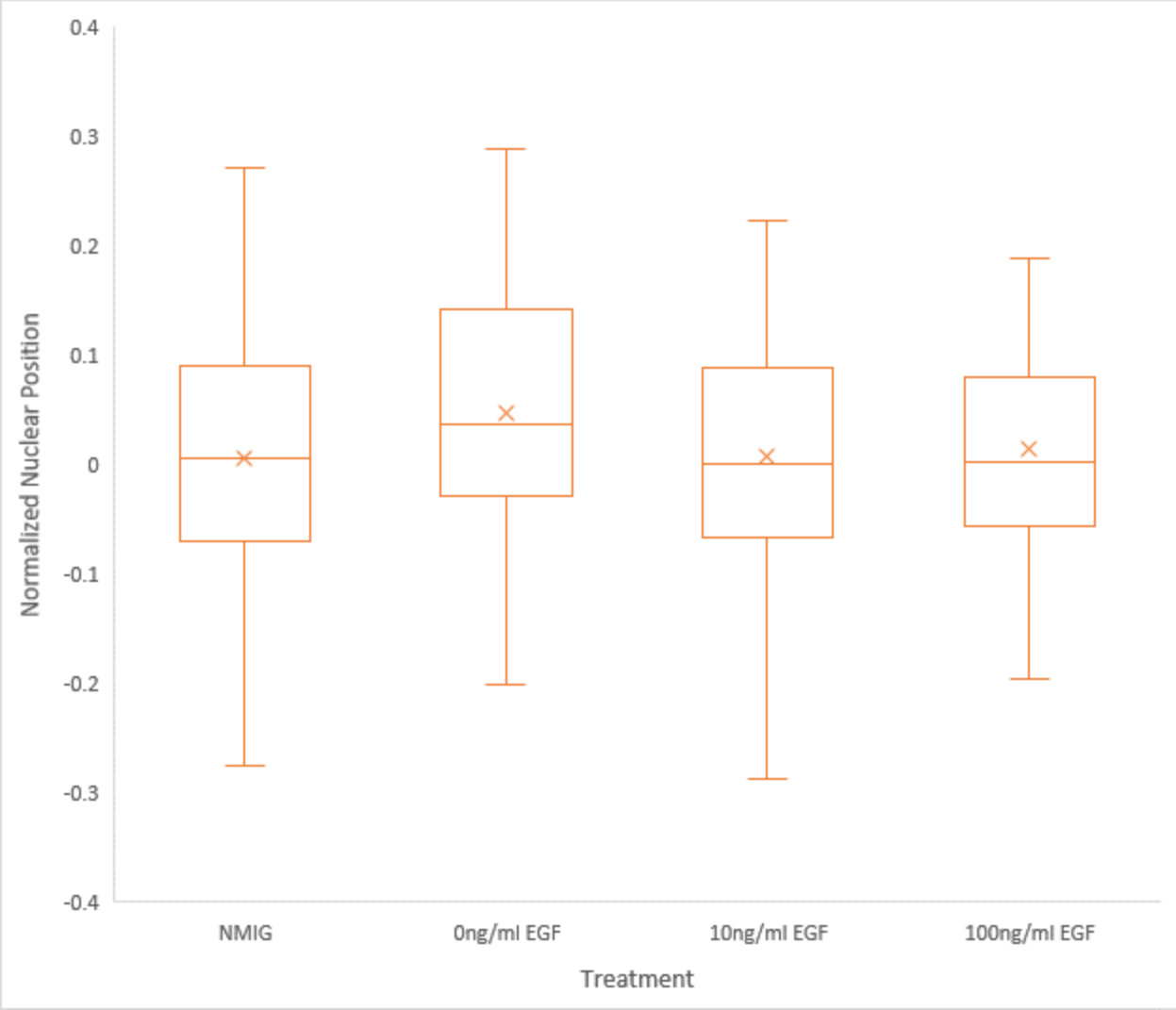

Figure 4. Nuclear positioning (NP) within non-migratory (NMIG, n=59) and migratory cells with increasing concentrations of EGF (0 ng/ml, n= 37; 10 ng/ml, n=67; 100 ng/ml, n=65). An NP of zero (0) represents a nucleus at center or midline of cell, positive values portray more anterior nuclei, and negative values represent more posterior nuclei. Average NP between all groups (NMIG= 0.0059, 0 ng/ml EGF= 0.0464, 10 ng/ml= 0.0067, 100 ng/ml= 0.0146) was not significantly different from another (ANOVA, $p > 0.05$).

Migration Upon Mitochondrial Distribution

The first goal of this study was to determine whether cellular migration induced redistribution of mitochondria within MDA-MB-231 cells. The first aim to achieve this goal was to compare mitochondria localization index (MLI) between non-migratory (NMIG) and migratory (MIG) cells in scratch assays. Figure 5 shows the percentage of cells within NMIG and MIG treatments displaying the mitochondria locations: posterior, peri-nuclear, and anterior. The percentage of mitochondria located in the anterior regions of NMIG (n = 59) and MIG (n = 38) cells were 39% and 42%, respectively (Figure 5). The percentage of mitochondria located in the posterior regions of NMIG and MIG cells were 37% and 42%, respectively (Figure 5). The percentage of mitochondria located in the peri-nuclear regions of NMIG and MIG cells were 24% and 16%, respectively (Figure 5). The induction of migration did not cause a significant redistribution in overall mitochondria localization (Contingency analysis, $p > 0.05$). Due to the variability seen in both groups, the average MLI of non-migratory and migratory cells were equal (0.54), thus not significant (Figure 6; Student's t-test, $p > 0.05$).

The data show there was no difference in the overall, whole-cell distribution of mitochondria between non-migratory and migratory cells. 39% of non-migratory and 42% of migratory cells displayed anterior locations (Figure 5). Of these cells which had mitochondria in anterior regions, average anterior MLI (Mean ± SD) between the two groups showed that mitochondria within migratory cells (0.95 ± 0.07) localized further into the anterior region than in non-migratory cell (0.88 ± 0.09) (Student's t-test, $p < 0.05$). Therefore, migration did not cause an overall shift of mitochondria to localize in anterior regions; yet, migration did cause mitochondria to localize further into the anterior regions within MDA-MB-231 cells.

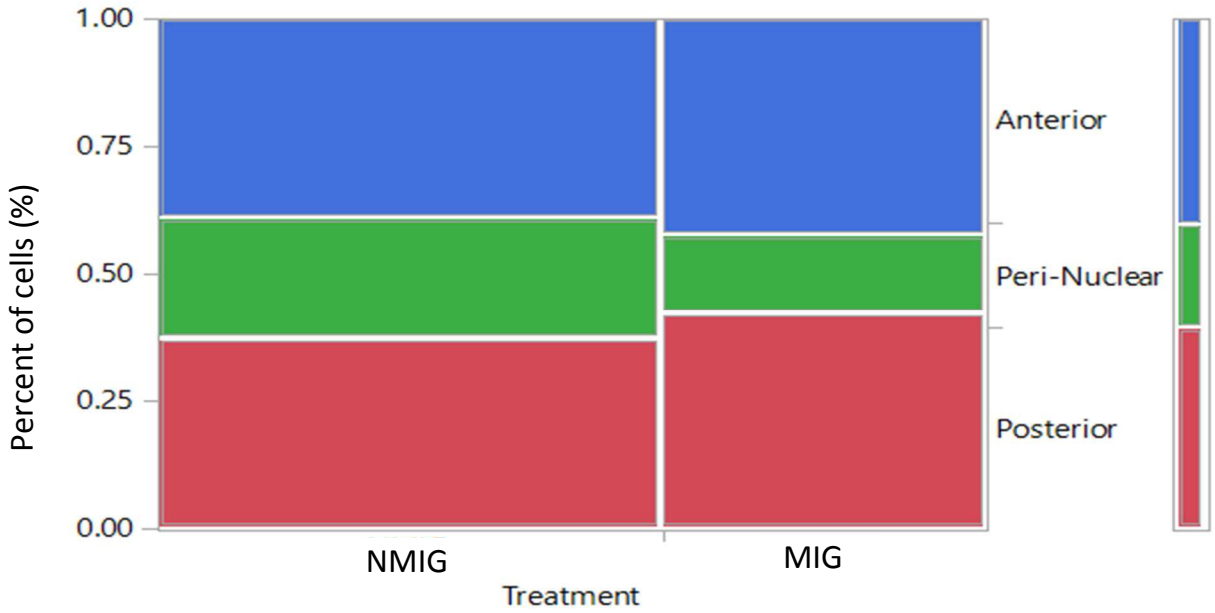

Figure 5. Distributions of non-migratory and migratory cells in terms of their mitochondrial localizations: anterior (blue), peri-nuclear (green), posterior (red). Within NMIG cells (n = 59), 37% show posterior mitochondria location, 24% peri-nuclear, and 39% anterior. Within MIG cells (n = 38), 42% show posterior, 16% peri-nuclear, and 42% anterior. Through a contingency analysis of observed vs. expected between the two treatment groups and their respective mitochondrial localizations, there is no significant difference (Contingency analysis, $p > 0.05$).

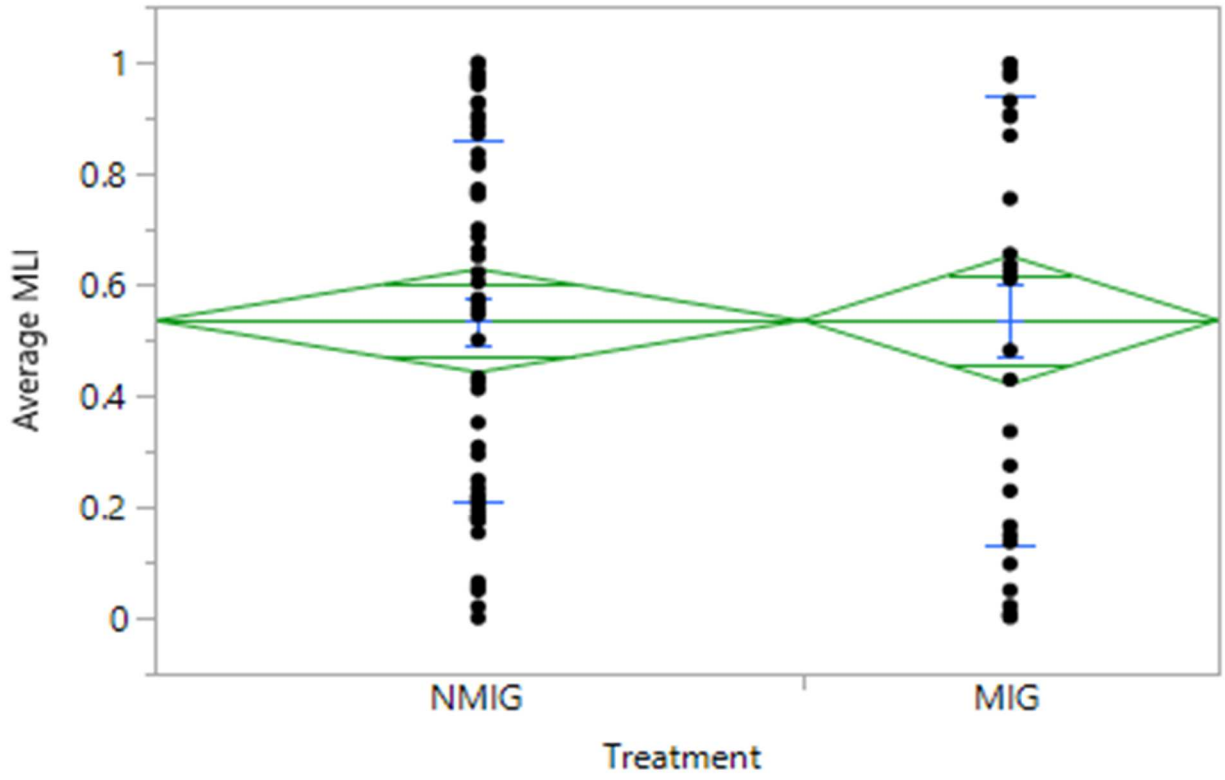

Figure 6. Average overall MLI compared between non-migratory (n = 59) and migratory cells (n = 38). Mean diamonds depict 95% confidence intervals, as well as upper and lower bounds to standard deviation (blue dashes). There was much variability within each group, thus average non-migratory MLI (0.54 ± 0.33) and migratory MLI (0.54 ± 0.40) were not found to be significant (Student's t-test, $p > 0.05$). Data are presented as mean ± SD.

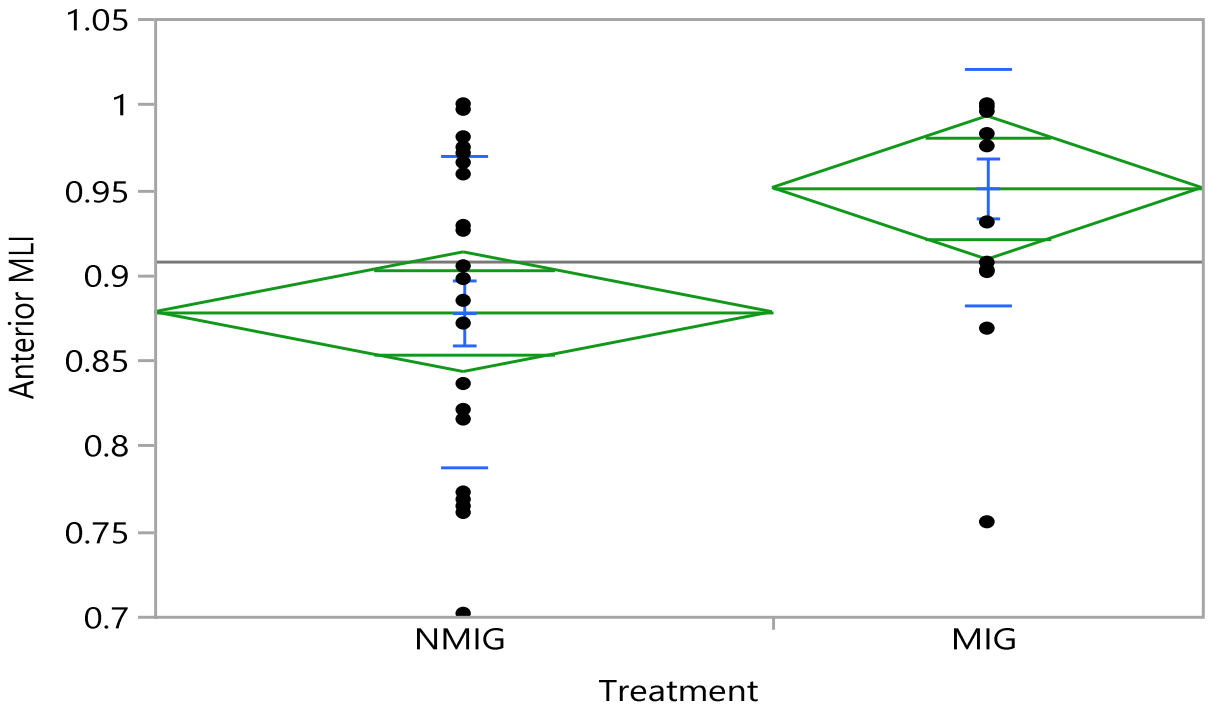

Figure 7. Average anterior MLI between non-migratory (n = 23) and migratory (n = 16) cells displaying mitochondria within the anterior regions of the cell. Mean diamonds depict 95% confidence intervals, as well as upper and lower bounds to standard deviation (blue dashes). NMIG cells show a larger spread of anterior locations and more variability within the data, whereas MIG cells seem to have most mitochondria further into the anterior regions. When compared to average NMIG MLI (0.88 ± 0.09), the average MIG MLI (0.95 ± 0.07) is significantly larger (Student's t-test, $p < 0.05$). Data are presented as mean ± SD.

Effect of EGF on Mitochondrial Distribution

Epidermal growth factor (EGF) had previously been shown to increase the rates of migration in MDA-MB-231 cells (Kim et al., 2016; Bell et al., 2017). The second aim for determining the redistribution of mitochondria in migratory cells, was determining the effect of increasing concentrations of EGF on mitochondrial localization index (MLI). Cells were treated with increasing concentrations of EGF: 0 ng/ml (Control, n = 38), 10 ng/ml (n = 67), and 100

ng/ml (n = 65). To determine whether EGF increases the overall location of mitochondria within migratory cells, average MLI was compared between each treatment (Figure 8). Cells treated with 10 ng/ml EGF were shown to have the highest average MLI (0.61 ± 0.35) however, compared to average MLI in 0 ng/ml (0.54 ± 0.40) and 100 ng/ml (0.58 ± 0.30), there was no significant difference (Student's t-test, $p > 0.05$).

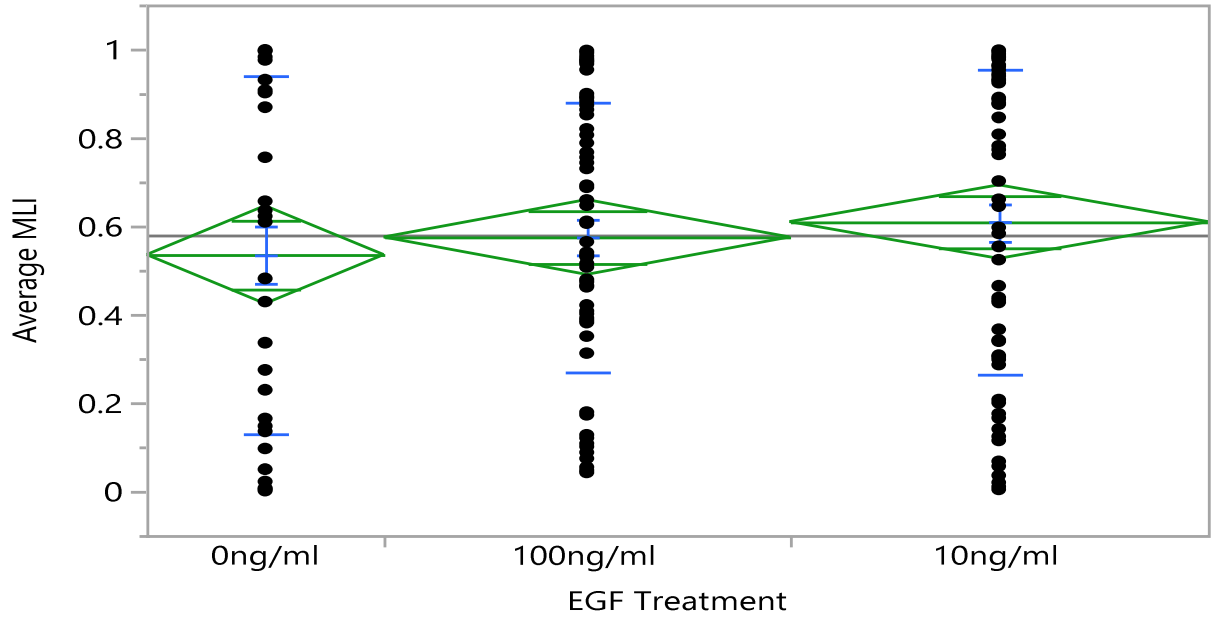

Figure 8. Average overall MLI between cells treated with increasing concentrations of EGF. Mean diamonds depict 95% confidence intervals, as well as upper and lower bounds to standard deviation (blue dashes). Cells treated with 10ng/ml EGF had the highest average MLI (0.61 ± 0.35). Comparing between 0 ng/ml (0.54 ± 0.40), 10 ng/ml, and 100 ng/ml (0.58 ± 0.30) there was no significant difference found (ANOVA, $p > 0.05$). Data are presented as mean ± SD.

Figure 9 shows the distributions of mitochondria within cells treated with EGF. As EGF concentration increased, there was a decrease in mitochondria localized in posterior regions (0 ng/ml = 42%; 10 ng/ml = 32%; 100 ng/ml = 23%), and an increase of localization within peri-nuclear (0 ng/ml = 16%; 10 ng/ml = 19%; 100 ng/ml = 39%) (Figure 9). The distribution of

mitochondria changed significantly as MLI was shown to be contingent upon concentration of EGF (Contingency analysis, $p<0.05$). Although these data did show that there was a shift of mitochondria from posterior to per-nuclear regions as EGF increased, among these groups there was no primary localization within anterior regions thus these data did not support the hypothesis that EGF causes mitochondria to primarily localize in anterior regions.

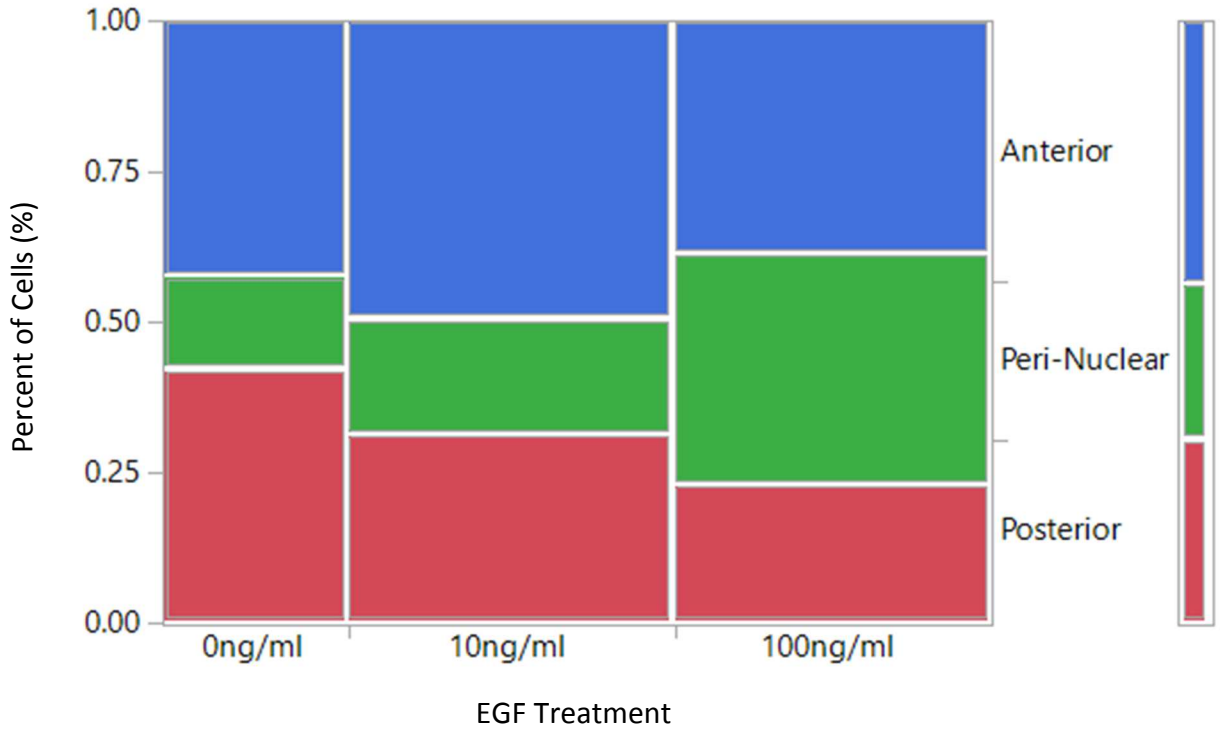

Figure 9. Distribution of mitochondria within cells treated with epidermal growth factor (EGF; ng/ml). Locations of mitochondria are grouped as posterior (blue), peri-nuclear (green), or anterior (red). Percentages of cells displaying the three locations are shown: anterior (0 ng/ml = 42%; 10 ng/ml = 49%; 100 ng/ml = 39%), peri-nuclear (0 ng/ml = 16%; 10 ng/ml = 19%; 100 ng/ml = 39%), and posterior (0 ng/ml = 42%; 10 ng/ml = 32%; 100 ng/ml = 23%). For total distributions of mitochondria within treatments, there is a significant difference among groups (Contingency analysis, $p < 0.05$).

However, as with the previous comparison between non-migratory and migratory cells, the comparison of overall, whole-cell mitochondrial distribution did not examine the extent to which the mitochondria localize into the leading edges. Thus, average anterior MLI across treatments were compared and differences of how far mitochondria localized within anterior regions was seen. Figure 10 shows there was significant difference in average anterior MLI as the concentration of EGF increased (ANOVA, $p = 0.05$). Furthermore, through a post-hoc Dunnett's test against control, where 0 ng/ml EGF was the defined control, there was found to be no significant difference between control and 10 ng/ml EGF ($p > 0.05$); yet, there was a significant difference between control and 100 ng/ml EGF ($p < 0.05$). Based on this data we could say there was an effect of EGF treatment upon anterior mitochondria location within MDA-MB-231 cells. As the concentration of EGF increased, there was a decrease in mitochondria localized in posterior regions. However, when examining the span of anterior mitochondrial locations between treatments, there was a decrease in anterior MLI as the concentration of EGF treatment increased. This was unexpected, as it suggested treatment of EGF decreased the extent to which mitochondria localized in anterior regions.

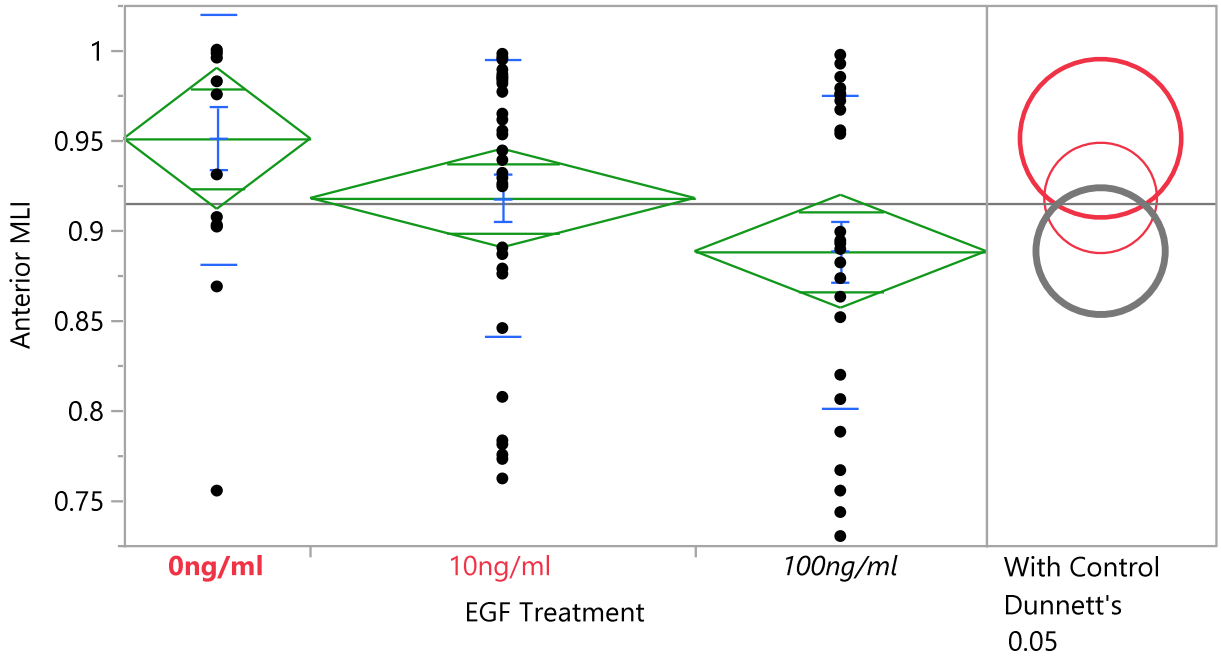

Figure 10. Comparison of Average anterior MLI across cells treated with increasing concentrations of epidermal growth factor (EGF, ng/ml). Mean diamonds depict 95% confidence intervals, as well as upper and lower bounds to standard deviation (blue dashes). Average anterior MLI (0 ng/ml, 0.95 ± 0.07; 10 ng/ml, 0.92 ± 0.08; 100 ng/ml, 0.89 ± 0.09) is seen to decrease as EGF concentration increases and groups were found to be significantly different (ANOVA, $p = 0.05$). Post-hoc Dunnett's test against control, with control defined as 0 ng/ml (bold red) was found not to be significantly different from 10ng/ml (red, $p > 0.05$), but significantly different from 100 ng/ml (grey, $p > 0.05$). Data are presented as mean ± SD.

MITOCHONDRIA MORPHOLOGY WITHIN MIGRATORY MDA-MB-231

The second goal of this study was to determine the dominant mitochondrial phenotype in migratory cells. To achieve this goal, the first aim was to determine if the phenotype differed between non-migratory and migratory cells. The second aim was determining the effect of EGF treatment upon phenotype localization in anterior regions. Z stack images from the localization studies were analyzed for mitochondrial phenotype between non-migratory cells and cells treated with increasing concentrations of EGF. Fluorescent mitochondria were observed in each

Maximum Intensity Projection image, and labelled linked (L), if they were fused tubular networks, or fissioned (F) if the organelles were fragmented (Figures 11).

The majority of non-migratory cells (64.4%) exhibited fused networks of mitochondria whereas the majority of migratory cells (65.8%) exhibited fissioned mitochondria (Figure 12; Fisher's exact, $p < 0.05$). This shows that a fissioned phenotype was contingent upon migration in these cells. Figure 13 shows the observed distributions of mitochondrial phenotype when location of phenotype was added. Location of phenotype was labelled according to presence in anterior regions of the cells, yes (Y) or no (N). Of all non-migratory cells (n = 59), 32.2% exhibited mitochondria present in anterior regions, and of migratory cells (n = 38), 60.5% displayed mitochondria present in the anterior region (Figure 13). The location of mitochondrial phenotypes was found to be contingent upon migration (Contingency analysis, $p < 0.05$). Migratory cells primarily display a fissioned mitochondrial phenotype and these fissioned mitochondria seem to be localizing mainly in anterior regions of migratory cells.

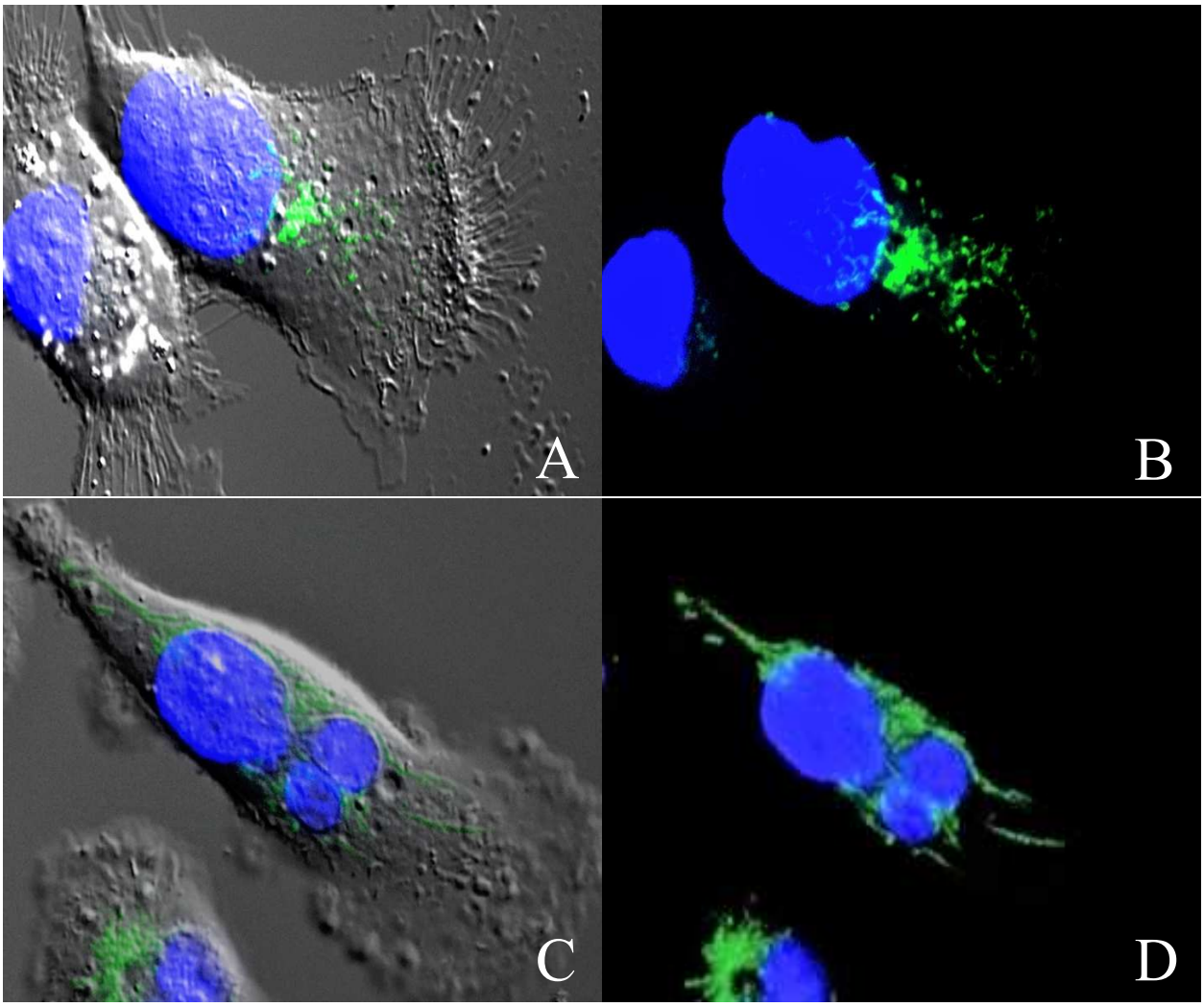

Figure 11. Images showing the two mitochondrial phenotypes within MDA-MB-231 cells. Fissioned mitochondria located within anterior region of a migrating cell (A and B). Fused tubular networks of mitochondria seen throughout a migratory cell (C and D). Panels A and C are a combination of DAPI, FITC, and transmitted light fluorescent channels. Panels B and D are the same cells as A and C, yet only shown through DAPI and FITC fluorescent channels.

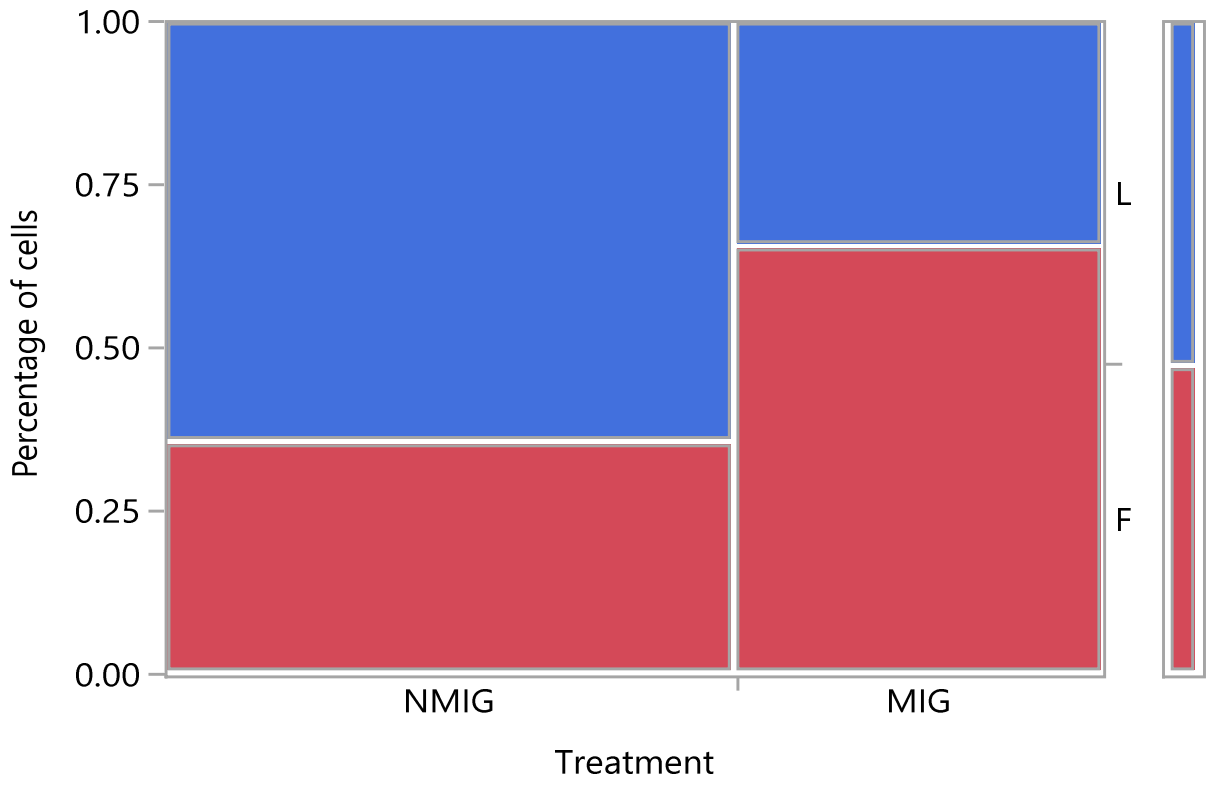

Figure 12. Comparison of mitochondrial phenotype between NMIG (n= 59) and MIG (n=38) cells. Mitochondria were labelled as linked (L) for a fused phenotype and fissioned (F) for a fragmented phenotype. There is a significant difference between cells displaying fissioned mitochondria in MIG cells compared to NMIG cells (Fisher's exact, $p < 0.05$).

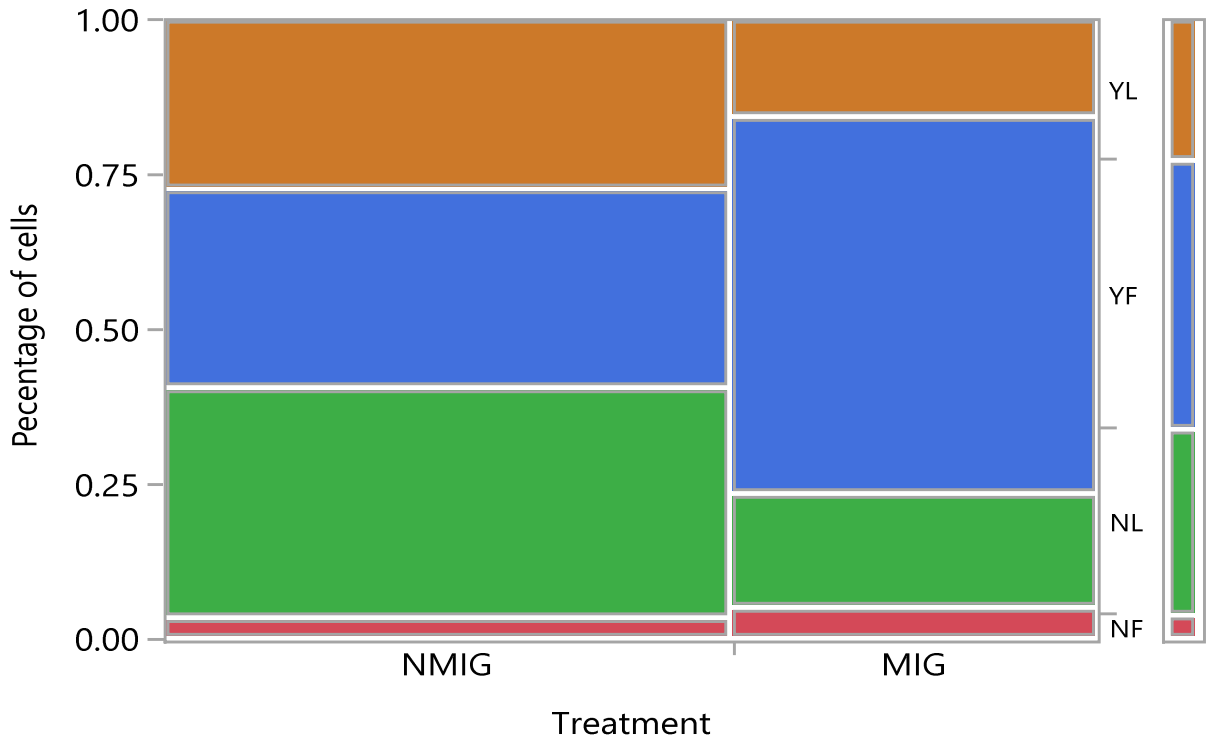

Figure 13. Observed distributions of mitochondrial phenotype and location of phenotype in NMIG and MIG cells. Mitochondria were labelled as linked (L) for a fused phenotype and fissioned (F) for a fragmented phenotype, as well as being present in anterior regions, yes (Y) or no (N). Location of phenotypes in NMIG cells were: 3.4% NF, 37.3% NL, 32.2% YF, and 27.1% YL. Location of phenotype in MIG cells were: 5.3% NF, 18.4% NL, 60.5% YF, and 15.8% YL. Percentages of phenotype location were found to be contingent upon migration (Contingency analysis, $p < 0.05$).

Figure 14 shows the observed distribution of mitochondrial phenotype throughout cells treated with increasing concentrations of epidermal growth factor (EGF; 0 ng/ml = Control, 10 ng/ml, and 100 ng/ml). All groups of migratory cells displayed primarily fissioned mitochondrial phenotypes (Control = 65.8%, 10 ng/ml = 80.6%, 100 ng/ml = 69.2%). This was not surprising as MIG cells previously displayed primarily fissioned phenotype (Figure 12). However, here mitochondrial phenotype was found to not be contingent upon EGF treatment (Contingency

analysis, $p > 0.05$). It may have been that specifically the act of migration was what was contingent with mitochondrial phenotype.

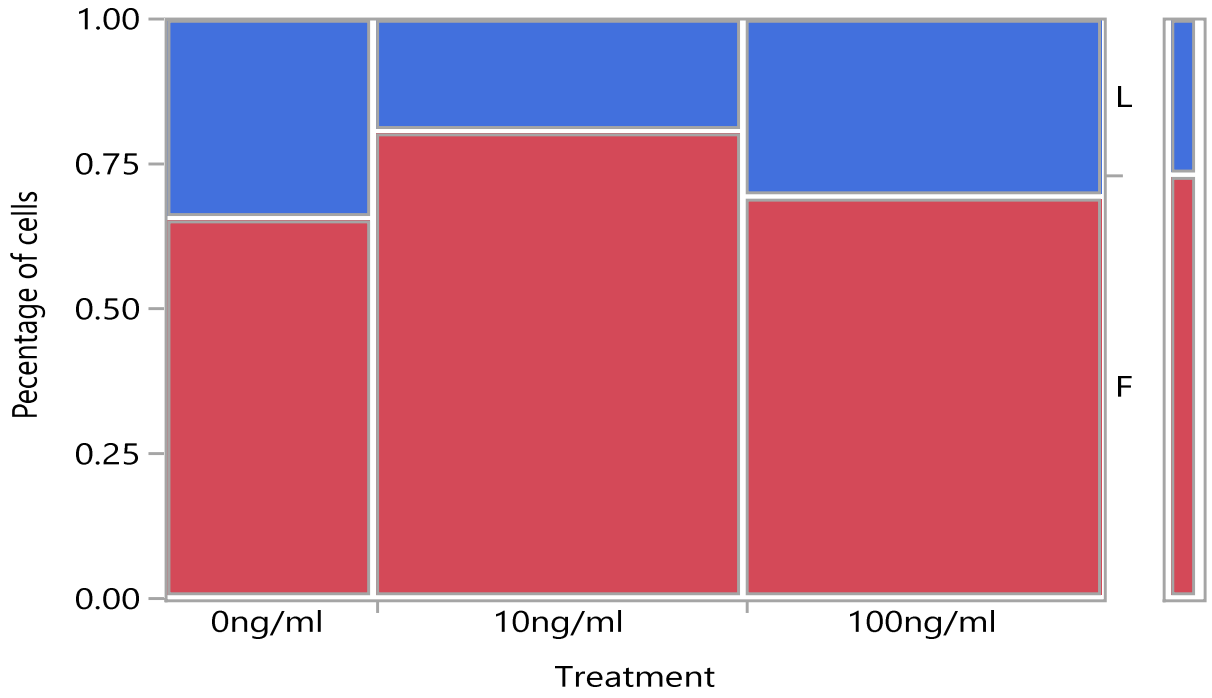

Figure 14. Observed distributions of mitochondrial phenotypes in cells treated with increasing concentrations of EGF (0 ng/ml= Control, 10 ng/ml, and 100 ng/ml). Fissioned phenotype dominates in all groups (Control = 65.8%, 10 ng/ml = 80.6%, 100 ng/ml = 69.2%). Percentage of cells displaying either phenotype was not contingent upon EGF treatment (Contingency analysis, $p > 0.05$).

Figure 15 shows the distributions of fissioned and fused mitochondria when also defined by presence of the phenotype in anterior region of the cell, yes (Y) or no (N). Between cells treated with EGF, there was a majority of fissioned mitochondria found within the anterior region (0 ng/ml = 60.5%, 10 ng/ml = 64.2%, and 100 ng/ml = 61.5%). However, EGF treatment was not found to be contingent upon where mitochondria phenotypes were locating. Again, it

may have been the act of migration which lead to a fissioned phenotype and the location of fissioned mitochondria in anterior regions, not the addition of EGF. These results are unexpected as EGF is known to increase rates of migration in MDA-MB-231 cells in a previous study by Bell et al. (2017), therefore it was predicted that EGF would increase the amount of fissioned mitochondria in anterior regions.

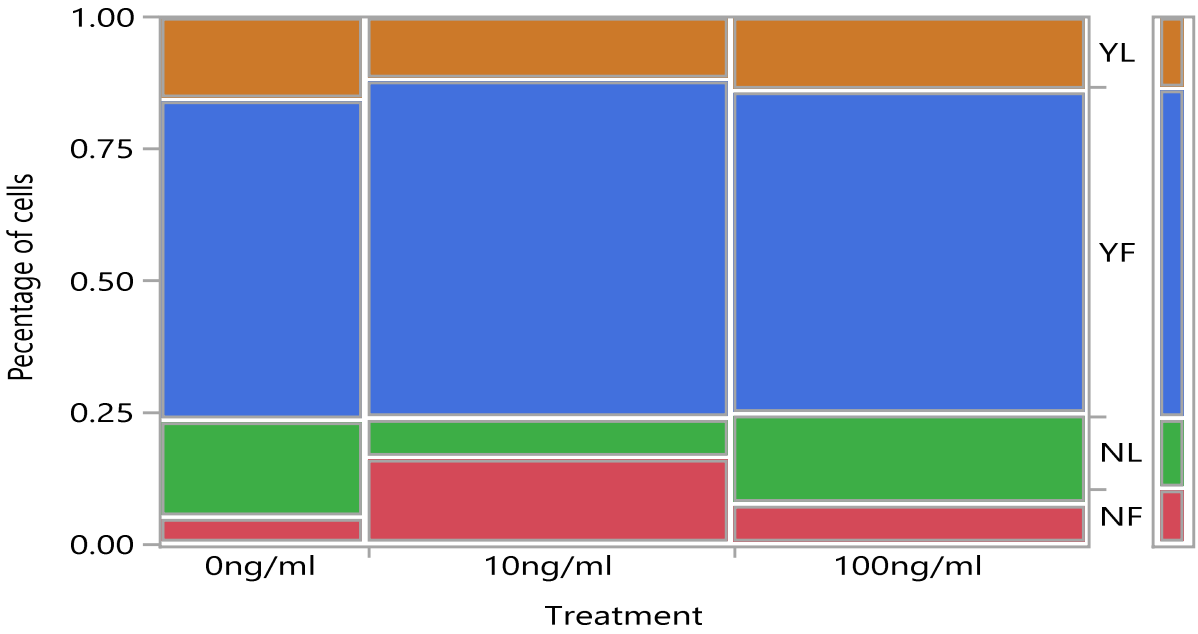

Figure 15. Observed distributions of mitochondrial phenotype and location of observed phenotype in cells treated with increasing concentrations of EGF. Mitochondria were labelled linked (L) or fissioned (F), in addition to presence within anterior regions, yes (Y) or no (N). Percentages of phenotype location in cells with Control (0 ng/ml) were: 5.3% NF, 18.4% NL, 60.5% YF, and 15.8% YL. In cells with treatment of 10 ng/ml EGF: 16.4% NF, 7.5% NL, 64.2% YF, and 11.9% YL. In cells with treatment of 100 ng/ml EGF: 7.7% NF, 16.9% NL, 61.5% YF, and 13.9% YL. Percentages of phenotype location was not found to be contingent upon EGF treatment (Contingency analysis, $p > 0.05$).

DOSAGE RESPONSE OF MDA-MB-231 TO SODIUM AZIDE DURING CELL MIGRATION

Sodium azide (NaN_3) decreases intracellular ATP production through oxidative phosphorylation by inhibiting cytochrome c oxidase in the electron transport chain. The third goal was to determine the effect of ETC inhibition upon cell migration to examine whether migratory MDA-MB-231. Migration rates of MDA-MB-231 cells were analyzed via scratch wound assay with treatment of increasing concentrations of NaN_3 (0.001-20 mM) compared to control (0 mM).

Assays of migration rates were first performed with NaN_3 concentrations ranging from 0-10 mM. Plates 1 and 2 (P1, P2) each contained two replicates of each concentration (n = 20 measurements/concentration/plate, n = 40 measurements total), and significant difference among treatments could be seen (Figure 16, ANOVA $p < 0.05$). Post-hoc Dunnett's test shows significant effect in cells treated with 10 mM NaN_3 compared to control (0 mM) ($p < 0.05$).

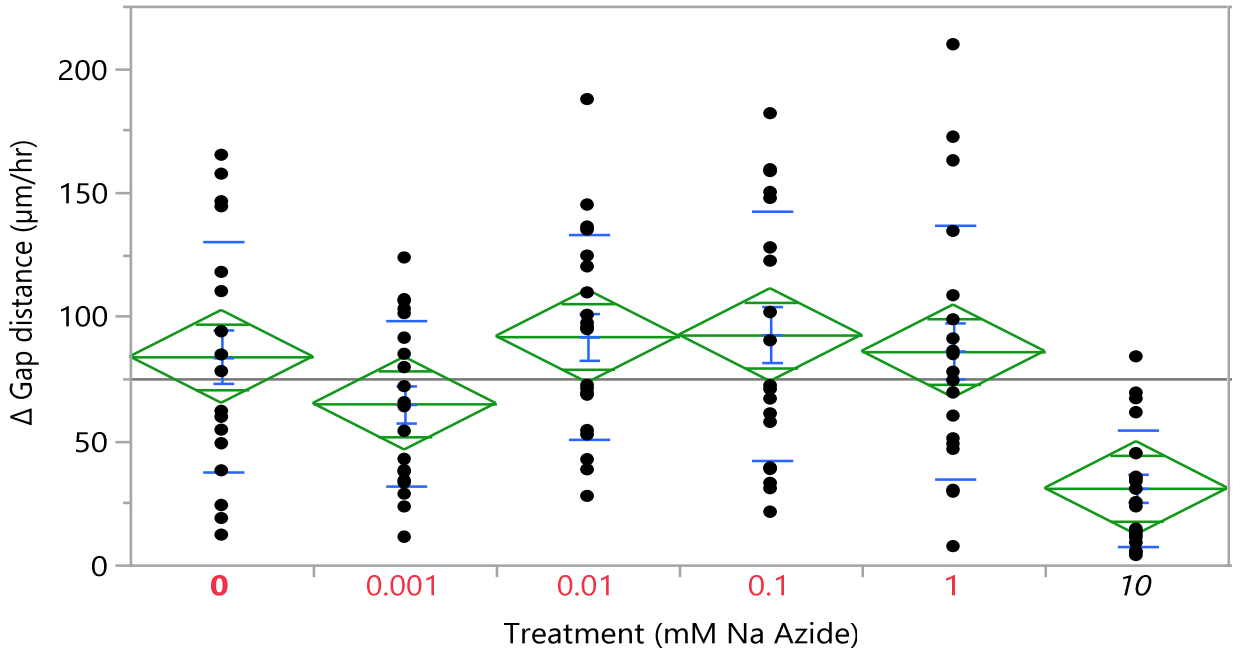

Figure 16. Analysis of migration as a change in gap distance among treatments in P1 and P2. Mean diamonds depict 95% confidence intervals, as well as upper and lower bounds to standard deviation (blue dashes). There were 20 samples/treatment. Significance was seen among treatments (ANOVA, $p < 0.05$). When comparisons are made against control (0 mM, bold red), significant difference was only seen in 10 mM treatment (Dunnett's test, $p < 0.05$).

The results from P1 and P2 prompted an additional assay to determine the effect of a concentration higher than 10 mM. Therefore, plate 3 (P3) was examined with a new, 20 mM treatment (Figure 17). However, there were no significant differences among treatments (ANOVA $p > 0.05$). A post-hoc Tukey-Kramer or Dunnett's was not performed due to non-significance.

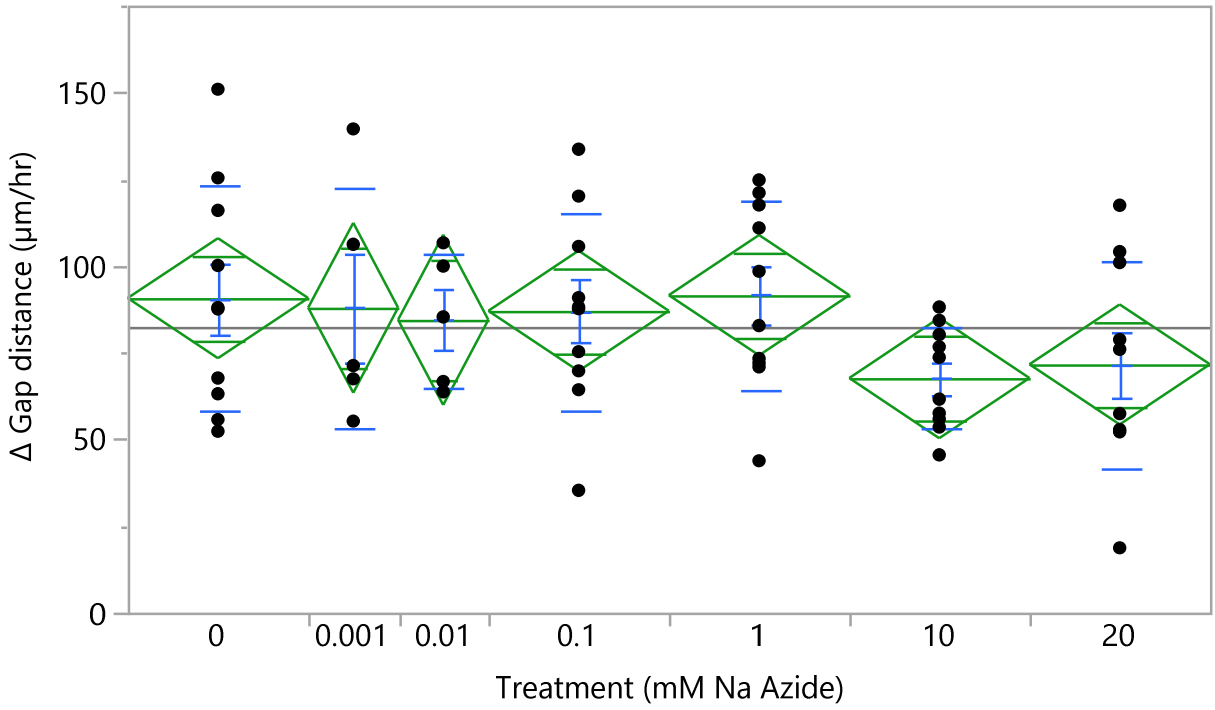

Figure 17. Analysis of migration rates among treatments in plate 3 (P3). Mean diamonds depict 95% confidence intervals, as well as upper and lower bounds to standard deviation (blue dashes). Sample size of 0.001 mM is n = 5, all other groups are 10 samples/treatment. Among treatments, there was no difference in mean Δ Gap distance (ANOVA, $p > 0.05$).

Results from P3 prompted additional assays utilizing even greater concentrations of NaN_3. Therefore, plates 4 and 5 (P4, P5) included an additional 100 mM NaN_3 treatment (Figure 18). Both P4 and P5 were 24-well plates with 4 replications of 5 concentrations (0, 0.1, 1, 10, and 100 mM NaN_3; n = 35 total measurements for control, n = 40 for all other treatments). Significant differences were seen among treatments (Welch's ANOVA, $p < 0.05$). Specific differences were seen where both 0 mM and 0.1 mM were significantly different from 1 mM, 10 mM, and 100 mM, as well as 1 mM being significantly different from both 10 mM and 100 mM

(Tukey-Kramer HSD, $p < 0.05$). No significant difference in migration rates were seen between 10 mM and 100 mM, or between 0 mM and 0.01 mM treatments (Tukey-Kramer HSD, $p > 0.05$). When treatment groups were compared to control (0 mM) there were significant differences in migration rates seen in 1 mM, 10 mM, and 100 mM (Dunnett's, $p < 0.05$).

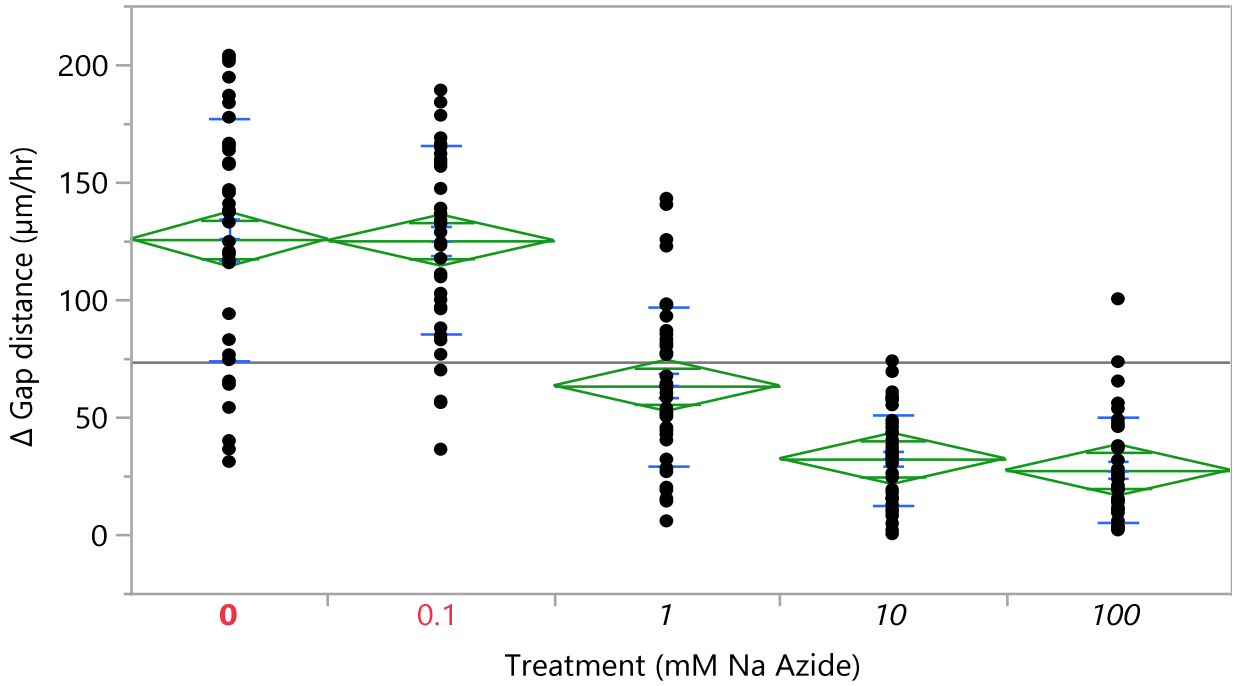

Figure 18. Analysis of migration rates among treatments in both plate 4 and 5 (P4, P5). Mean diamonds depict 95% confidence intervals, as well as upper and lower bounds to standard deviation (blue dashes). Sample size of 0 mM is n = 15, all other groups are 20 sample/treatment. Significant difference in rates was seen among treatments (Welch's ANOVA, $p < 0.05$). Post-hoc Tukey-Kramer HSD shows that 0 mM and 0.1 mM (red) are significantly different from 1 mM, 10 mM, and 100 mM (black, $p < 0.05$) with further difference in 1 mM from both 10 mM and 100 mM ($p < 0.05$). Post-hoc Dunnett's test shows significance in 1 mM, 10 mM, and 100 mM (black) when compared to Control (0 mM, bold red).

All treatments (0.001-100 mM, excluding 20mM) from all plates (P1-P5) were combined (Figure 19). Samples of 20 mM NaN_3 were excluded due to not following a ten-fold increase of the previous concentration, thus it was believed that 20 mM is not representing a true effect of an increase in NaN_3 treatment on migration rates. Although among samples from P3 showed 10 mM NaN_3 was not significantly different (Figure 17), there was no plate effect seen (Two-way ANOVA, $p > 0.05$). When compared to control (0 mM) migration rates, significant differences were seen in cells treated with 0.001, 1, 10, and 100 mM NaN_3 (Dunnett's, $p < 0.05$). Surprisingly, there was a significant difference in 0.01mM and 0.1mM compared to 0.001 mM ($p < 0.05$). With this surprising result, migration rates were shown to increase when NaN_3 concentrations increased from 0.001 to 0.01 mM and 0.1 mM, then rates lowered significantly when cells were treated with 1 mM, 10 mM, and 100 mM NaN_3. To verify that the effects seen of NaN_3 on migration were not a product of cell death, a post-hoc trypan exclusion assay revealed that no concentration of NaN_3 was toxic to the cells, with cell viability never below 90%. Thus, the rates from migration observed among treatment groups were because of NaN_3 and not to cell death.

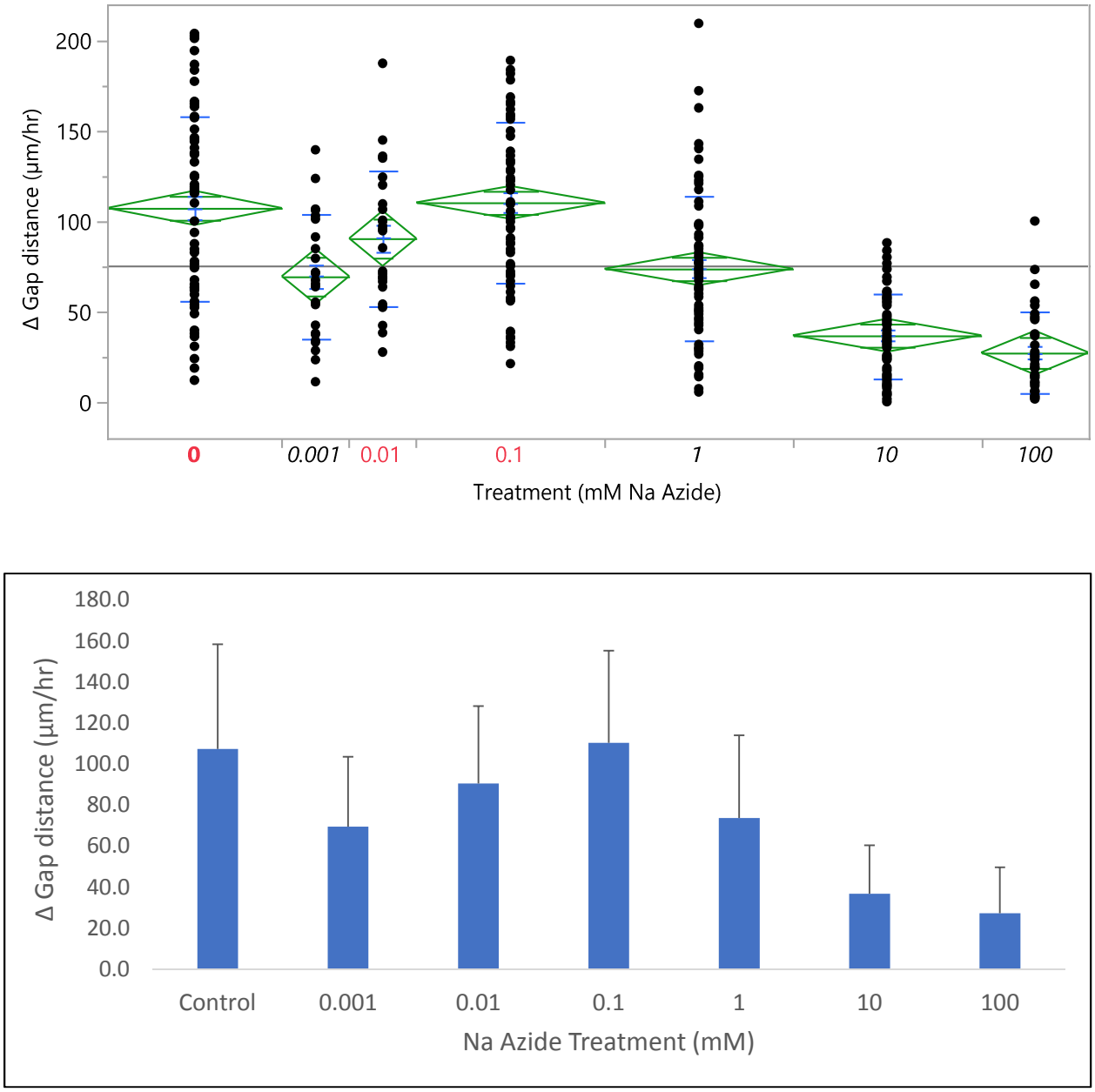

Figure 19. (Top) Analysis of migration rates among all treatments, excluding 20 mM, between all plates (P1-P5). Mean diamonds depict 95% confidence intervals, as well as upper and lower bounds to standard deviation (blue dashes). (Bottom) Bar graph displaying of Δ Gap Distance among NaN_3 treatments, excluding 20mM. Error bars on top of columns represents standard deviation (SD). Sample size of treatments: 0 mM (n = 65), 0.001 and 0.01 mM (n = 25), 0.1, 1, and 10 mM (n = 70), 100 mM (n = 40). Significant difference was seen among treatments (Welch's ANOVA, $p < 0.05$). Compared to mean control rate (0 mM, 107.39 ± 50.93) significantly different Δ Gap Distance was seen in treatments: 0.001 mM (69.54 ± 34.11, $p < 0.05$), 1 mM (73.77 ± 40.26, $p < 0.05$), 10 mM (36.89 ± 23.56, $p < 0.05$), and 100 mM (27.33 ± 22.47, $p < 0.05$). Data are presented as mean ± SD.

RESAZURIN ASSAY UPON MITOCHONDRIAL ACTIVITY

Resazurin is commonly used as a sensitive assay to measure mitochondrial activity in living cells. When the cell's mitochondria are metabolically active, blue and non-fluorescent resazurin will be broken down into resorufin, a pink fluorescent compound. The fluorescent intensity of resorufin could be measured among cells treated with the increasing concentrations of sodium azide to verify that sodium azide is inhibiting mitochondria.

Among groups of cells pretreated with increasing sodium azide concentrations there was a significant difference in mitochondrial activity, as analyzed through differences among the slopes of the treatment groups (Figure 20; Repeated Measures ANOVA, $p < 0.05$). Post-hoc comparisons against Control (0 mM) exhibited significant difference in 100 mM NaN_3 (Dunnett's, $p < 0.05$). Furthermore, significant comparisons were seen between all treatment groups and 100 mM (Tukey-Kramer HSD, $p < 0.05$). These data show that at least at the highest dose of NaN_3 (100 mM) treatment there was a significant decrease in mitochondrial activity. This decrease in ETC activity at 100 mM could explain the decrease in migration observed at the 100 mM NaN_3 treatment (Figure 19).

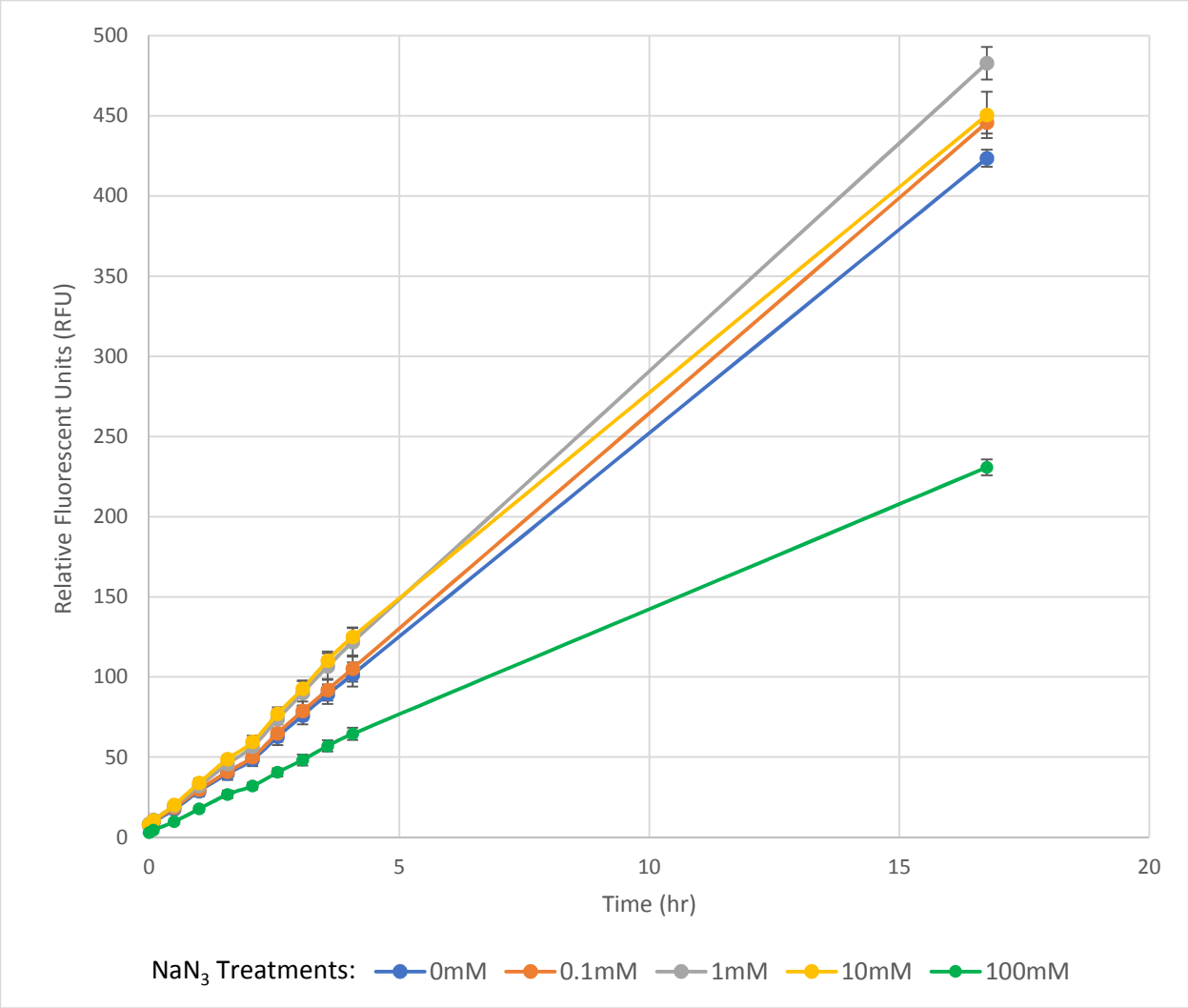

Figure 20. Resorufin fluorescence over time in cells treated with increasing concentrations of sodium azide (0-100 mM) as a measure of mitochondrial activity. A significant effect between time and treatment upon RFU was seen (Repeated Measures ANOVA, $p < 0.05$). 100 mM NaN_3 treatment groups was shown to have significantly lower RFU compared to all other treatment groups (Tukey-Kramer HSD, $p < 0.05$), Furthermore, comparing Control (0 mM) rate across treatments, significant difference was seen only in the 100 mM treatment group (Dunnett's, $p < 0.05$).

CHAPTER V: DISCUSSION

MDA-MB-231 cells utilize the Warburg effect, an altered metabolism in which glycolysis is enhanced, and pyruvate is preferentially converted into lactate despite the availability of oxygen in the environment. Although glycolysis is enhanced during the Warburg effect, there is no significant increase in ATP synthesis compared to oxidative phosphorylation in normal cells (Shestov et al., 2014). The Warburg effect increases utilization of glycolytic intermediate, glucose-6-phosphate, in the pentose phosphate pathway (PPP) to convert $NADP^+$ into NADPH and create ribose-5-phosphate needed for nucleotide synthesis. Furthermore, with the use of glycolysis for anabolism, the intermediate glyceraldehyde-3-phosphate is converted into glycerol-3-phosphate for use in the synthesis of lipids. Cancer cells utilize this altered metabolism to meet anabolic requirements for rapid growth and proliferation, suggesting use of electron transport chain (ETC) and oxidative phosphorylation is diminished. However, cellular migration is an energy expensive process that requires catabolism and utilization of abundant ATP rather than nucleotide and lipid synthesis. Thus, MDA-MB-231 cells may utilize a metabolic switch from the Warburg effect to cellular respiration for efficient ATP synthesis necessary in cellular migration, similar to the metabolic switch seen in pancreatic ductal adenocarcinoma (PDAC) (Rozeveld et al., 2019).

MDA-MB-231 cells may be utilizing the Warburg effect specifically for anabolic metabolism to facilitate rapid growth and proliferation based upon studies of how glioblastoma utilize the Warburg effect metabolism (DeBerardinis et al., 2007) and the increased use of pentose phosphate pathway (Yang et al., 2018). During cellular migration, actin dynamics drives protrusion of lamellipodia and requires hydrolysis of ATP to elongate actin filaments. Mitochondria have been shown to localize within anterior lamellipodia of glioma and breast

cancer cells and cause an increase in velocity and persistence of migration as well as invasion in vitro through trans well inserts (Arismendi-Morillo et al., 2012, Desai et al., 2013, Zhao et al., 2013). The work done by Desai et al. (2013) utilized microfluidics devices to deliver epidermal growth factor (EGF) for the initiation of cellular migration, and Intensity Profiles for the quantification of mitochondria location. Z stack images allow for the observation and quantification of mitochondria thorughout the three dimensional cell, as opposed to the two dimensional line scan of Intensity Profiles. With a z stack image, a region of interest (ROI) can be drawn around a cell and the fluorescent mitochondria. The ROIs can then be used to determine Sum Intensity levels of all fluorescent mitochondria and group them according to the three MLI groups: posterior (MLI 0-0.35), peri-nuclear (0.35-0.70), and anterior (0.70-1.00). The first goal of this thesis was to determine if cellular migration was associated with a redistribution of mitochondria in MDA-MB-231 cells with a first specific aim of determining if migration caused a redistribution of mitochondria and compared MLI between non-migratory and migratory cells. When overall MLI was compared between non-migratory and migratory cells, there was no significant difference in observed mitochondrial location from expected distributions (Figure 5), as well as no difference between average whole-cell MLI (Figure 6). This opposed the thought that mitochondria primarily localize in anterior regions of migratory MDA-MB-231 cells. However, the majority of sampled migratory cells which displayed anterior MLI showed that most mitochondria localize in the extremity of anterior regions than in non-migratory cells displaying anterior MLI (Figure 7). These data may support the notion that mitochondria in migratory cells may be supplying the leading edge with ATP for actin dynamics.

The second specific aim of determining mitochondrial redistribution was to examine if treatment of increasing concentrations of epidermal growth factor (EGF) affected localization.

EGF has a profound impact on increasing rate of migration within MDA-MB-231 cells (Kim et al., 2016, Bell et al., 2017). The chemoattractant was also used in Desai et al. (2013) (100 ng/ml EGF) for inducing MDA-MB-231 cellular migration. Average MLI between groups showed that EGF did not cause a primary anterior mitochondrial localization, and treatment groups were not significantly different from Control (Figure 8). When breaking down the groups to compare the distributions of mitochondria within the cells, there was shown to be a significant redistribution of mitochondria as EGF concentration increased (Figure 9). However, of the migratory cells displaying anterior localizations, EGF treatment caused a decrease in the distance to the leading edge that mitochondria would localize (Figure 10). Thus, EGF did not cause mitochondria to localize primarily in anterior regions, but it did cause the cells to issue a significant redistribution of mitochondria throughout the cell.

Mitochondria are dynamic organelles capable of displaying two phenotypes: fused and fissioned (Chen & Chan, 2017). Fused mitochondria are incapable of being trafficked and this phenotype is mainly used for mtDNA maintenance and mitigating cell stress (Chen et al., 2005; Farmer et al., 2018; Westermann, 2012). A fissioned mitochondrial phenotype allows for organelle trafficking to areas of high ADP:ATP ratios (Cunniff et al., 2016, Schuler et al., 2017). Thus, fissioned mitochondria are necessary for increased migration and may allow for anterior localization of the organelle. The second goal of this study was to determine the dominant mitochondrial phenotype in migratory cells, with the first aim being to determine if the phenotype differed between non-migratory and migratory cells, and the second aim being to determine the effect of EGF treatment upon phenotype localization in anterior regions. Qualitative comparison of mitochondria morphology between non-migratory cells, and migratory cells showed that a fissioned phenotype was dominant within migratory cells, but a fused

network phenotype was dominant in non-migratory cells (Figure 12). Furthermore, of migratory cells displaying the fissioned phenotype, these mitochondria were primarily seen in anterior regions (Figure 13). Treatments of EGF did show a dominance of a fissioned mitochondrial phenotype, however there was no effect of EGF on anterior localization of fissioned mitochondria (Figures 14, 15). The data do not refute previous work by Zhao et al. (2013) but do suggest an extension upon the notion that MDA-MB-231 cells show a primarily fissioned phenotype, where it is the anterior regions of migratory MDA-MB-231 cells where the fissioned phenotype dominates. Overall, these data do not support the primary anterior localization of mitochondria during migration as shown by Desai et al. (2013). The effects of migration and EGF upon mitochondrial location may require use of time lapse visualization for more effective determination. The distribution of mitochondria may be a dynamic process as a cell migrates, and time lapse visualization may have the capability of displaying the primary anterior distributions which could not be determined in this study.

Cellular migration is an energy expensive process, where efficient ATP production through oxidative phosphorylation may best provide ATP for actin dynamics. The Warburg effect decreases oxidative phosphorylation (Fantin et al., 2006; Shim et al., 1997) to provide more substrates necessary for biomass production (Yang et al., 2018). To examine whether migratory MDA-MB-231 cells depend upon oxidative phosphorylation, the third goal is to determine the effect of ETC inhibition upon cell migration in scratch wound assays. Sodium azide (NaN_3) is a known complex IV inhibitor of ETC, causing a build-up of reduced substrates and decrease in proton pumping and ATP sythesis (Tsubaki and Yoshikawa 1993, Schwoebel et al., 2002). Anterior localization of fissioned mitochondria suggests cells may use mitochondria to supply leading edges with ATP for actin dynamics. Thus inhibition of ETC may affect cellular

migration. Here we showed that treatment of NaN_3 at concentrations of 0.001, 1, 10, and 100 mM significantly reduced MDA-MB-231 cellular migration rates, but did not halt migration completely (Figure 19). In addition to an effect upon migration seen with treatments of 0.001, 1, 10, and 100 mM NaN_3, resazurin reduction assay only showed an inhibitory effect upon mitochondrial activity in cells pretreated with 100 mM NaN_3 (Figure 20). This result may have been due to the resazurin assay not being sensitive enough to have shown an effect among cells treated with low NaN_3 concentrations. The inhibiton of ETC with 100 mM NaN_3 slows migration and mitochondrial activity significantly, suggesting ATP production through oxidative phosphorylation is important for migration.

In future studies, it would be pertinent to use time lapse videos when quantifiying mitochondria location among EGF treatments. It may be that mitochnodria area trafficked back and forth from nucelus to lamelipodia, which time lapse videos would capture. More research is needed to determine the slowed rate of migration seen with NaN_3 concentrations 0.001, 1, and 10 mM in order to clarify the variability seen in the resazurin assay. Furthermore, NADH/FAD autofluorescence and/or lactate dehydrogenase assays may be useful in quantification of oxidative phosphorylation during MDA-MB-231 cellular migration.

In this thesis, we showed that all mitochondria within migratory did not primarily localize in anterior regions, and treatment of EGF decreased the extent to which the mitochondria penetrate into anterior regions. However, despite where overall mitochondria may have localized in migratory cells, the mitochondria which have a fissioned phenotype localized primarily in anterior regions. In addition, we showed that ATP produced via the ETC was important for MDA-MB-231 cell migration, as the inhibition of ETC with 100 mM NaN_3 reduced migration rates and mitochondrial activity. The data shown did not definitively show a metabolic switch

occuring, but did show that MDA-MB-231 cell migration may lessen the need for the Warburg effect through employment of oxidative phosphorylation during migration, mitigated by trafficking fissioned mitochondria to leading edges.

LITERATURE CITED

Adekola, K., Rosen, S. T., & Shanmugam, M. (2012). Glucose transporters in cancer metabolism. *Current Opinion in Oncology*, *24*(6), 650–654. https://doi.org/10.1097/CCO.0b013e328356da72

Alberts, B., Johnson, A., Lewis, J., Morgan, D., Raff, M., Roberts, K., & Walter, P. (2015). *Molecular Biology of the Cell* (6th ed.). Garland Science.

Arismendi-Morillo, G., Hoa, N. T., Ge, L., & Jadus, M. R. (2012). Mitochondrial network in Glioma's invadopodia displays an activated state both in situ and in vitro: Potential functional implications. *Ultrastructural Pathology*, *36*(6), 409–414. https://doi.org/10.3109/01913123.2012.694582

Bell, B., Zahn, L., Grady, C., Lundin-Schiller, S. Comparison of migration rates and microtubule nucleation in MDA-MB-231 and MCF-7 breast cancer cells. Annual Meeting of The American Society for Cell Biology/European Molecular Biology Organization, Philadelphia, PA. 2017. (Poster).

Caino, M. C., Ghosh, J. C., Chae, Y. C., Vaira, V., Rivadeneira, D. B., Faversani, A., … Altieri, D. C. (2015). PI3K therapy reprograms mitochondrial trafficking to fuel tumor cell invasion. *Proceedings of the National Academy of Sciences*, *112*(28), 8638–8643. https://doi.org/10.1073/pnas.1500722112

Cancer.net. (2019). Breast Cancer: Statistics. Retrieved March 11, 2019, from https://www.cancer.net/cancer-types/breast-cancer/statistics/2015

Cancer.org. (n.d.). Tamoxifen and raloxifene for breast cancer prevention. https://doi.org/10.2165/00128413-200113120-00009

Chen, H., & Chan, D. C. (2017). Mitochondrial Dynamics in Regulating the Unique Phenotypes of Cancer and Stem Cells. *Cell Metabolism*, *26*(1), 39–48. https://doi.org/10.1016/j.cmet.2017.05.016

Chen, H., Chomyn, A., & Chan, D. C. (2005). Disruption of Fusion Results in Mitochondrial Heterogeneity and Dysfunction. *Journal of Biological Chemistry, 280(*28), 26185-26192. https://doi.org/10.1074/jbc.M503062200

Chen, H., Detmer, S. A., Ewald, A. J., Griffin, E. E., Fraser, S. E., & Chan, D. C. (2003). Mitofusins Mfn1 and Mfn2 coordinately regulate mitochondrial fusion and are essential for embryonic development. *Journal of Cell Biology*, *160*(2), 189–200. https://doi.org/10.1083/jcb.200211046

Chi, Q., Yin, T., Gregersen, H., Deng, X., Fan, Y., Zhao, J., … Wang, G. (2014). Rear actomyosin contractility-driven directional cell migration in three-dimensional matrices: A mechanochemical coupling mechanism. *Journal of the Royal Society Interface*, *11*(95). https://doi.org/10.1098/rsif.2013.1072

Cipolat, S., De Brito, O. M., Dal Zilio, B., & Scorrano, L. (2004). OPA1 requires mitofusin 1 to promote mitochondrial fusion. *Proceedings of the National Academy of Sciences of the United States of America*, *101*(45), 15927–15932. https://doi.org/10.1073/pnas.0407043101

Cunniff, B., McKenzie, A. J., Heintz, N. H., & Howe, A. K. (2016). AMPK activity regulates

trafficking of mitochondria to the leading edge during cell migration and matrix invasion. *Molecular Biology of the Cell*, *27*(17), 2662–2674. https://doi.org/10.1091/mbc.e16-05-0286

Dai, X., Cheng, H., Bai, Z., & Li, J. (2017). Breast Cancer Cell Line Classification and Its Relevance with Breast Tumor Subtyping. *Journal of Cancer*, *8*(16), 3131–3141. https://doi.org/10.7150/jca.18457

DeBerardinis, R. J., Mancuso, A., Daikhin, E., Nissim, I., Yudkoff, M., Wehrli, S., & Thompson, C. B. (2007). Beyond aerobic glycolysis: Transformed cells can engage in glutamine metabolism that exceeds the requirement for protein and nucleotide synthesis. *Proceedings of the National Academy of Sciences of the United States of America*, *104*(49), 19345–19350. https://doi.org/10.1073/pnas.0709747104

Desai, S. P., Bhatia, S. N., Toner, M., & Irimia, D. (2013). Mitochondrial localization and the persistent migration of epithelial cancer cells. *Biophysical Journal*, *104*(9), 2077–2088. https://doi.org/10.1016/j.bpj.2013.03.025

Fantin, V. R., St-Pierre, J., & Leder, P. (2006). Attenuation of LDH-A expression uncovers a link between glycolysis, mitochondrial physiology, and tumor maintenance. *Cancer Cell*, *9*(6), 425–434. https://doi.org/10.1016/j.ccr.2006.04.023

Farmer, T., Naslavsky, N., & Caplan, S. (2018, August 1). Tying trafficking to fusion and fission at the mighty mitochondria. *Traffic*, Vol. 19, pp. 569–577. https://doi.org/10.1111/tra.12573

Friedman, J. R., Lackner, L. L., West, M., DiBenedetto, J. R., Nunnari, J., & Voeltz, G. K. (2011). ER tubules mark sites of mitochondrial division. *Science*, *334*(6054), 358–362. https://doi.org/10.1126/science.1207385

Gatenby, R. A., & Gillies, R. J. (2004). Why do cancers have high aerobic glycolysis? *Nature Reviews Cancer*, *4*(11), 891–899. https://doi.org/10.1038/nrc1478

Guise, T. (2010). Examining the Metastatic Niche : Targeting the Microenvironment. *Seminars in Oncology*, *37*(5), S2–S14. https://doi.org/10.1053/j.seminoncol.2010.10.007

Han, T., Kang, D., Ji, D., Wang, X., Zhan, W., Fu, M., … Wang, J. Bin. (2013). How does cancer cell metabolism affect tumor migration and invasion? *Cell Adhesion and Migration*, *7*(5), 395–403. https://doi.org/10.4161/cam.26345

Ibrahim, T., Leong, I., Sanchez-sweatman, O., Khokha, R., Sodek, J., Tenenbaum, H. C., … Cheifetz, S. (2000). Expression of bone sialoprotein and osteopontin in breast cancer bone metastases. *Clinical and Experimental Metastasis, 18,* 253–260.

Jin, L., & Zhou, Y. (2019). Crucial role of the pentose phosphate pathway in malignant tumors (review). *Oncology Letters*, *17*(5), 4213–4221. https://doi.org/10.3892/ol.2019.10112

Kim, J., Kong, J., Chang, H., Kim, H., & Kim, A. (2016). EGF induces epithelial-mesenchymal transition through phospho-Smad2/3-Snail signaling pathway in breast cancer cells. *Oncotarget*, *7*(51), 85021–85032. https://doi.org/10.18632/oncotarget.13116

Korn, E. D., Carlier, M.-F., & Pantaloni, D. (1987). Actin Polymerization and Hydrolysis. *Science*, *238*, 638–644.

Krakhmal, N. V., Zavyalova, M. V., Denisov, E. V., Vtorushin, S. V., & Perelmuter, V. M. (2015). Cancer invasion: Patterns and mechanisms. *Acta Naturae*, *7*(2), 17–28.

Kurosaka, S., & Kashina, A. (2008). Cell biology of embryonic migration. *Birth Defects Research Part C - Embryo Today: Reviews*, *84*(2), 102–122. https://doi.org/10.1002/bdrc.20125

Langley, R. R., & Fidler, I. J. (2011). The seed and soil hypothesis revisited--the role of tumor-stroma interactions in metastasis to different organs. *International Journal of Cancer*, *128*(11), 2527–2535. https://doi.org/10.1002/ijc.26031

Lee, J. E., Westrate, L. M., Wu, H., Page, C., & Voeltz, G. K. (2016). Multiple dynamin family members collaborate to drive mitochondrial division. *Nature*, *540*(7631), 139–143. https://doi.org/10.1038/nature20555

Liberti, M. V., & Locasale, J. W. (2016, March 1). The Warburg Effect: How Does it Benefit Cancer Cells? *Trends in Biochemical Sciences*, Vol. 41, pp. 211–218. https://doi.org/10.1016/j.tibs.2015.12.001

Losó n, O. C., Song, Z., Chen, H., & Chan, D. C. (2013). Fis1, Mff, MiD49, and MiD51 mediate Drp1 recruitment in mitochondrial fission. *Molecular Biology of the Cell*, *24*(5), 659–667. https://doi.org/10.1091/mbc.E12-10-0721

MacVicar, T., & Langer, T. (2016). OPA1 processing in cell death and disease - the long and short of it. *Journal of Cell Science*, *129*(12), 2297–2306. https://doi.org/10.1242/jcs.159186

Matoba, S., Kang, J. G., Patino, W. D., Wragg, A., Boehm, M., Gavrilova, O., … Hwang, P. M. (2006). P53 Regulates Mitochondrial Respiration. *Science*, *312*(5780), 1650–1653. https://doi.org/10.1126/science.1126863

Narendra, D., Tanaka, A., Suen, D.-F., & Youle, R. J. (2009). *Parkin-induced mitophagy in the pathogenesis of Parkinson disease*. https://doi.org/10.4161/auto.5.5.8505

Nazarali, S. A., Narod, S. A., & Narod, S. (2014). *BCTT-43763-tamoxifen-for-healthy-women-at-high-risk-of-breast-cancer*. https://doi.org/10.2147/BCTT.S43763

Okimura, C., Taniguchi, A., Nonaka, S., & Iwadate, Y. (2018). Rotation of stress fibers as a single wheel in migrating fish keratocytes. *Scientific Reports*, *8*(1), 1–10. https://doi.org/10.1038/s41598-018-28875-z

Paget, S. (1889). Distribution of secondary growths in cancer of the breast. *The Lancet*, *133*(3421), 571–573. https://doi.org/10.1007/s12307-014-0163-5

Pagliuso, A., Cossart, P., & Stavru, F. (2018, February 1). The ever-growing complexity of the mitochondrial fission machinery. *Cellular and Molecular Life Sciences*, Vol. 75, pp. 355–374. https://doi.org/10.1007/s00018-017-2603-0

Poincloux, R., Collin, O., Lizárraga, F., Romao, M., Debray, M., Piel, M., & Chavrier, P. (2011). Contractility of the cell rear drives invasion of breast tumor cells in 3D Matrigel. *Proceedings of the National Academy of Sciences of the United States of America*, *108*(5), 1943–1948. https://doi.org/10.1073/pnas.1010396108

Robey, I. F., Stephen, R. M., Brown, K. S., Baggett, B. K., Gatenby, R. A., & Gillies, R. J.

(2008). Regulation of the Warburg effect in early-passage breast cancer cells. *Neoplasia*, *10*(8), 745–756. https://doi.org/10.1593/neo.07724

Rosania, G. R., & Swanson, J. A. (1996). Microtubules can modulate pseudopod activity from a distance inside macrophages. *Cell Motility and the Cytoskeleton*, *34*(3), 230–245. https://doi.org/10.1002/(SICI)1097-0169(1996)34:3<230::AID-CM6>3.0.CO;2-D

Rozeveld, C., Schulze, R., Zhang, L., & Razidlo, G. L. (2019). Abstract PR09: KRas modulates pancreatic cancer cell metabolism and invasive potential through the lipase HSL. *Cancer Research*, *79*(24 Supplement), PR09 LP-PR09. https://doi.org/10.1158/1538-7445.PANCA19-PR09

Schuler, M.-H., Cunniff, B., Kirchhausen, T., Upadhyayula, S., Skillern, W., Caprio, G. Di, … Shaw, J. M. (2017). Miro1-mediated mitochondrial positioning shapes intracellular energy gradients required for cell migration. *Molecular Biology of the Cell*, *28*(16), 2159–2169. https://doi.org/10.1091/mbc.e16-10-0741

Schwoebel, E. D., Ho, T. H., & Moore, M. S. (2002). The mechanism of inhibition of Ran-dependent nuclear transport by cellular ATP depletion. *Journal of Cell Biology*, *157*(6), 963–974. https://doi.org/10.1083/jcb.200111077

Senft, D., & Ronai, Z. A. (2016, April 1). Regulators of mitochondrial dynamics in cancer. *Current Opinion in Cell Biology*, Vol. 39, pp. 43–52. https://doi.org/10.1016/j.ceb.2016.02.001

Shestov, A. A., Liu, X., Ser, Z., Cluntun, A. A., Hung, Y. P., Huang, L., … Locasale, J. W. (2014). Quantitative determinants of aerobic glycolysis identify flux through the enzyme GAPDH as a limiting step. *ELife*, *3*(July2014), 1–18. https://doi.org/10.7554/eLife.03342

Shim, H., Dolde, C., Lewis, B. C., Wu, C.-S., Dang, G., Jungmann, R. A., … Dang, C. V. (1997). c-Myc transactivation of LDH-A: Implications for tumor metabolism and growth (oncogenelactate dehydrogenasehypoxiatumorigenicity). In *National Institutes of Health* (Vol. 94).

Silva Ramos, E., Larsson, N. G., & Mourier, A. (2016). Bioenergetic roles of mitochondrial fusion. *Biochimica et Biophysica Acta - Bioenergetics*, *1857*(8), 1277–1283. https://doi.org/10.1016/j.bbabio.2016.04.002

Singer, K., Kastenberger, M., Gottfried, E., Hammerschmied, C. G., Büttner, M., Aigner, M., … Kreutz, M. (2011). Warburg phenotype in renal cell carcinoma: High expression of glucose-transporter 1 (GLUT-1) correlates with low CD8+ T-cell infiltration in the tumor. *International Journal of Cancer*, *128*(9), 2085–2095. https://doi.org/10.1002/ijc.25543

Smelser, A. M., Macosko, J. C., O'Dell, A. P., Smyre, S., Bonin, K., & Holzwarth, G. (2015). Mechanical properties of normal versus cancerous breast cells. *Biomechanics and Modeling in Mechanobiology*, *14*(6), 1335. https://doi.org/10.1007/S10237-015-0677-X

Smirnova, E., Griparic, L., Shurland, D. L., & Van der Bliek, A. M. (2001). Dynamin-related protein Drp1 is required for mitochondrial division in mammalian cells. *Molecular Biology of the Cell*, *12*(8), 2245–2256. https://doi.org/10.1091/mbc.12.8.2245

Toschi, A., Lee, E., Thompson, S., Gadir, N., Yellen, P., Drain, C. M., … Foster, D. A. (2010).

Phospholipase D-mTOR requirement for the Warburg effect in human cancer cells. *Cancer Letters*, *299*(1), 72–79. https://doi.org/10.1016/j.canlet.2010.08.006

Tsubaki, M., & Yoshikawa, S. (1993). Fourier-Transform Infrared Study of Azide Binding to the Fe a3 -Cu B Binuclear Site of Bovine Heart Cytochrome c Oxidase: New Evidence for a Redox-Linked Conformational Change at the Binuclear Site. *Biochemistry*, *32*(1), 174–182. https://doi.org/10.1021/bi00052a023

Vander Heiden, M. G., Cantley, L. C., & Thompson, C. B. (2009). Understanding the Warburg Effect: The Metabolic Requirements of Cell Proliferation. *Science*, *324*(5930), 1029–1033. https://doi.org/10.1126/science.1160809.Understanding

Vicente-Manzanares, M. (2005). Cell migration at a glance. *Journal of Cell Science*, *118*(21), 4917–4919. https://doi.org/10.1242/jcs.02662

Warburg, O. (1956). On the origin of cancer cells. *Science*, *123*(3191), 309–314.

Westermann, B. (2012). Bioenergetic role of mitochondrial fusion and fission. *Biochimica et Biophysica Acta - Bioenergetics*, *1817*(10), 1833–1838. https://doi.org/10.1016/j.bbabio.2012.02.033

Yang, X., Peng, X., & Huang, J. (2018). Inhibiting 6-phosphogluconate dehydrogenase selectively targets breast cancer through AMPK activation. *Clinical and Translational Oncology*, *20*(9), 1145–1152. https://doi.org/10.1007/s12094-018-1833-4

Zhang, T.-B., Zhao, Y., Tong, Z.-X., & Guan, Y.-F. (2015). Inhibition of glucose-transporter 1 (GLUT-1) expression reversed Warburg effect in gastric cancer cell MKN45. In *Int J Clin Exp Med* (Vol. 8). Retrieved from www.ijcem.com/

Zhao, J., Zhang, J., Yu, M., Xie, Y., Huang, Y., Wolff, D. W., … Tu, Y. (2013). Mitochondrial dynamics regulates migration and invasion of breast cancer cells. *Oncogene*, *32*(40), 4814–4824. https://doi.org/10.1038/onc.2012.494